Structure and function of the EDEM:PDI ERAD checkpoint complex

Charlie J. Hitchman[1,2,11,13*], Andrea Lia[1,3,13], Gabriela N. Chiritoiu[4], Cristian V. A. Munteanu[4], Juan R. Ortigosa[5,6], Simona Ghenea[4], Christos Savva[1], Ikuo Wada[7], Maria De Benedictis[3], Gabor Tax[1,8,9], Yusupha Bayo[10,11], Irene Crescioli[10], Dominic L. Alonzi[12], Andrew Quigley[2], Carlos P. Modenutti[5,6,10], Stefana M. Petrescu[4], Angelo Santino[3*], Bibek Gooptu[1,2,13*], Nobuko Hosokawa[14*], Pietro Roversi[1,10*]

[1]Leicester Institute of Chemical and Structural Biology and Department of Molecular and Cell Biology, University of Leicester, Henry Wellcome Building, Lancaster Road, Leicester, LE1 7HR, United Kingdom.
[2]Membrane Protein Laboratory, Diamond Light Source Ltd., Research Complex at Harwell (RCaH), Harwell Science and Innovation Campus, Didcot, OX11 0DE, United Kingdom.
[3]Institute of Sciences of Food Production, C.N.R. Unit of Lecce, via Monteroni, Lecce, I-73100, Italy.
[4]Department of Molecular Cell Biology, Institute of Biochemistry, Romanian Academy, Splaiul Independentei 296, Bucharest, 060031, Romania.
[5]Departamento de Química Biológica, Facultad de Ciencias Exactas y Naturales, Universidad de Buenos Aires, Ciudad Universitaria, Pab. II, Buenos Aires, CE1428EHA, Argentina.
[6]Instituto de Química Biológica de la Facultad de Ciencias Exactas y Naturales (IQUIBICEN) CONICET, Ciudad Universitaria, Pab. II, Buenos Aires, CE1428EHA, Argentina.
[7]Department of Cell Sciences, Institute of Biomedical Sciences, Fukushima Medical University School of Medicine, Fukushima, 960-1295, Japan.
[8]Children's Cancer Institute, Lowy Cancer Research Centre, UNSW Sydney, Sydney, NSW, 2052, Australia.
[9]School of Clinical Medicine, UNSW Sydney, Sydney, NSW, 2052, Australia.

[10]Institute of Agricultural Biology and Biotechnology, IBBA-CNR Unit of Milano, via Bassini 15, Milano, I-20133, Italy.
[11]Department of Biosciences, University of Milano, via Celoria 26, Milano, I-20133, Italy.
[12]Centre for Teaching and Learning, University of Oxford, Littlegate House, 16-17 St Ebbe's Street, Oxford, OX1 1PT, United Kingdom.
[13]Department of Respiratory Sciences, University of Leicester, Glenfield Hospital, Leicester, LE3 9QP, United Kingdom.
[14]Laboratory of Molecular and Cellular Biology, Institute for Frontier Life and Medical Sciences, Kyoto University, Kyoto, 606-8507, Japan.
[15]These authors contributed equally to this work.

*Corresponding author(s). E-mail(s): chitchman@tulane.edu; angelo.santino@ispa.cnr.it; bg129@leicester.ac.uk; nobukoh3849@gmail.com; pietro.roversi@cnr.it;

Abstract

The ERAD glycoprotein misfolding checkpoint complex de-mannosylates misfolded glycoproteins to enable retrotranslocation, ubiquitination, and proteasomal degradation. The complex comprises an Endoplasmic Reticulum-Degradation Enhancing $\boldsymbol{\alpha}$-Mannosidase (EDEM) and a Protein Disulfide Isomerase (PDI). We solved Cryo-EM structures of *Chaetomium thermophilum (Ct) Ct*EDEM:*Ct*PDI, both as the heterodimer with no client and in complex with $\boldsymbol{\alpha}$1-antitrypsin (A1AT-NHK). The EDEM catalytic domain nests within the PDI arc, while A1AT-NHK binds EDEM's C-terminal flexible domains. Mass spectrometry reveals a disulfide bond between A1AT-NHK and an exposed Cys in the PAD of the EDEM. Co-transfection of EDEM, A1AT-NHK, and PDI shifts EDEM:PDI to higher molecular weight in non-reducing SDS-PAGE. Redox chemistry between EDEM and PDI disulfide bonds generates oxidized, demannosylation-competent EDEM and reduced PDI, priming PDI to function as the ERAD reductase, facilitating client retrotranslocation.

Keywords: ERAD, EDEM, PDI, CryoEM, A1AT-NHK, EDEM3, ERp46

Introduction

The tangled mess that forms when headphone wires are stuffed into a pocket is a familiar, everyday example of entropy at work on objects with an excess of degrees of freedom. Freshly translated glycopolypeptides trying to fold in the endoplasmic reticulum (ER) of eukaryotic cells also have many degrees of freedom, and although they face much stricter folding controls than headphone wires — they, too, can end up

in a tangled mess. Even worse: unlike headphone wires, which are topologically linear, glycoproteins often include disulfide bonds; when native cysteine pairings fail to form, a glycoprotein can adopt a nonlinear topology and become terminally misfolded.

Terminally misfolded glycoproteins are degraded by ER-associated degradation (ERAD [1–4] ERAD of pathogenic mutant glycoproteins relieves ER stress and alleviates acute proteostatic challenges, although it underpins pathogenic loss-of-function phenotypes [5–8]). When glycoprotein misfolding within the ER overwhelms ER degradation capacity, the ER stress response is triggered [9]. Persistent misfolded proteins not processed by ERAD are prone to toxic aggregation [10, 11]. Prolonged ER stress is a major mediator of chronic disease [12, 13].

ERAD detection of terminal glycoprotein misfolding is effected by ERAD checkpoint complexes [4, 14], each of which comprises an Endoplasmic Reticulum-Degradation Enhancing α-Mannosidase (EDEM) and a Protein Disulfide Isomerase (PDI). EDEM activity flags a terminally misfolded glycoprotein for degradation, by selective N-linked glycan demannosylation [15–18]. Once an EDEM has removed the outer mannose from the C branch of an N-glycan (see Supplementary Figure S1), the de-mannosylated glycoprotein proceeds to ERAD [18, 19] after recruitment by either the OS-9/Yos9/*At*OS9 or XTP3-B lectins, both of which are associated with the ERAD retrotranslocon [18, 20]. Through the latter, each EDEM-demannosylated glycoprotein is exported to the cytoplasm, where it is ubiquitinated and eventually digested by a proteasome [21–24].

The ERAD misfolded glycoprotein checkpoint was first discovered in *Saccharomyces cerevisiae* (*Sc*) as the disulfide-bonded *Sc*Mnl1(Htm1):*Sc*Pdi1 heterodimer [15, 25–28]. The heterodimeric nature of the ERAD misfolding checkpoint complex is functionally conserved across eukaryotes. In particular, each of the three mammalian EDEM paralogues (namely EDEM1, 2 and 3 [29–32]) forms an ERAD checkpoint complex with its own partner PDI family member: EDEM1:ERdj5 [33, 34]; EDEM2:TXNDC11 [17, 35, 36]; and EDEM3:ERp46 [37]. Despite the centrality of glycoprotein degradation to ER proteostasis [14, 38–40], the molecular determinants of misfolded glycoprotein recognition and de-mannosylation by the EDEM:PDI ERAD checkpoint complexes remain elusive.

We report here the Cryo-EM structure of an EDEM:PDI complex from the thermophilic yeast *Chaetomium thermophilum* (*Ct*). The *Ct*EDEM:*Ct*PDI structure provides the structural basis for branch C glycan specificity in EDEMs, and confirms that EDEM and PDI are covalently linked by two disulfide bonds, each between a free Cys on the EDEM with the first Cys of one of the PDI CXXC redox motifs. A low resolution Cryo-EM reconstruction of the *Ct*EDEM:*Ct*PDI complex with a classic ERAD substrate, the $\text{Null}_{\text{HongKong}}$ variant of α1-antitrypsin (A1AT-NHK) indicates that the EDEM flexible C-terminal domains are involved in client recognition, likely through interaction with exposed hydrophobic surfaces. Biochemical data suggest that disulfide redox chemistry as well as mediating complex formation, is essential for substrate recognition and enzyme activation.

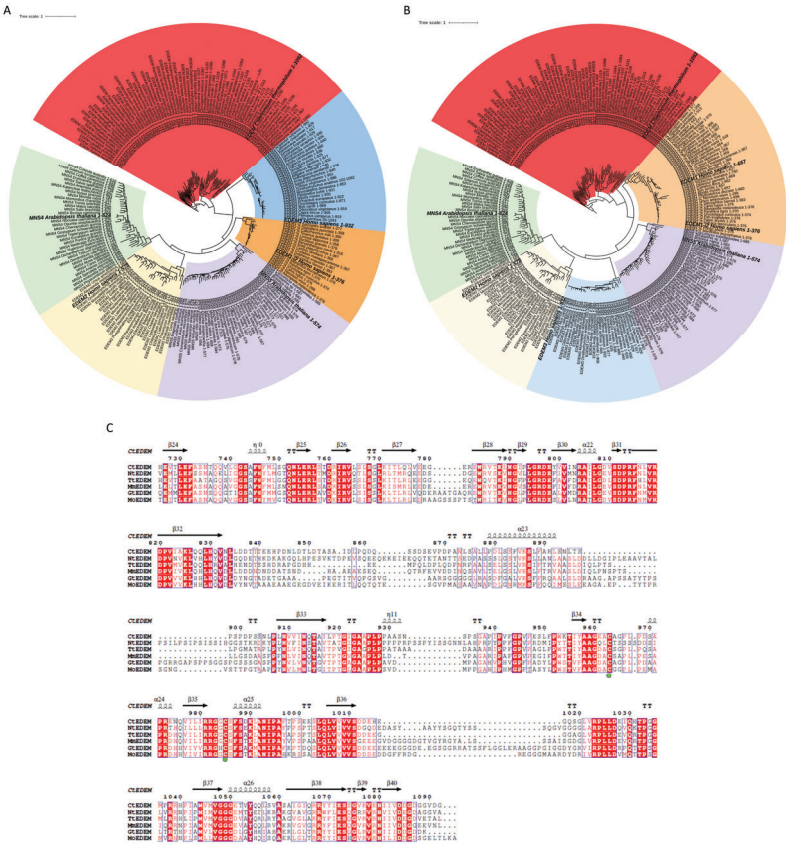

Fig. 1 EDEM phylogeny and C-terminal fungal EDEM domains A: Structure-based EDEMs phylogenetic tree; **B**: Sequence-based EDEMs phylogenetic tree; **C**: alignment of sequences of C-terminal intermediate domain (IMD) and protease-associated domain (PAD) tandems of fungal EDEMs. The Cys residues in the conserved disulfide bond at *Ct*EDEM Cys963:Cys985 are labelled with two green dots. *Ct*EDEM: *Chaetomium thermophilum*, Uniprot G0SCX7 · G0SCX7_CHATD; *Nt*EDEM: α-1,2-Mannosidase *Neurospora tetrasperma*, Uniprot F8N2I2 · F8N2I2_NEUT8; *Tt*EDEM: α-1,2-Mannosidase *Thermothielavioides terrestris*, Uniprot A0A3S4EST0 · A0A3S4EST0_9PEZI; *Mm*EDEM: α-1,2-Mannosidase *Madurella mycetomatis*, Uniprot A0A175VNQ1 · A0A175VNQ1_9PEZI; *Gt*EDEM: α-1,2-Mannosidase *Gaeumannomyces tritici*, Uniprot J3NGG5 · J3NGG5_GAET3; *Mo*EDEM: α-1,2-Mannosidase *Magnaporthe oryzae*, Uniprot G4NB03 · G4NB03_MAGO7.

Results

Mammalian EDEM1s and EDEM3s pre-date EDEM2s

All EDEMs include a domain belonging to the Glycosyl Hydrolase 47 (GH47) α-1,2-mannosidase family of enzymes. As well as the catalytic domains of EDEMs, the

GH47 fold family also comprises ER Man I and other Golgi α-mannosidases [41][1]. In unicellular eukaryotes, only one EDEM gene is present [43]; plants have two genes annotated as EDEMs (MNS4 and MNS5) [44]; metazoans have three [45]. To elucidate the evolutionary relationships between EDEM proteins, we deployed structure-based and sequence-based phylogeny [46, 47], analyzing unicellular eukaryotic EDEMs, plant MNS4s and MNS5s, and mammalian EDEMs, with the initial sequence sets and models taken from the `AlphaFold Clusters` repository (https://cluster.foldseek.com/, Supplementary Figure S2) [48].

Figures 1A and B illustrate the EDEMs phylogenetic tree coming from structure-based and sequence-based phylogeny, respectively [46, 47]. Using the former approach, six branches emerge from the analysis, differing in sequence regions outside the GH47 domain:

1. unicellular eukaryotic EDEMs (red branch in Figure 1A): these proteins feature an N-terminal membrane associated region, a GH47 domain followed by a linker region, and two distinct C-terminal domains, which we call Intermediate Domain (IMD) and protease associated domain (PAD) - in keeping with the nomenclature established for mammalian EDEM3 in [49]. Figure 1C illustrates the alignment of a few fungal EDEM IMD-PADs sequences; the C-terminal domain contains a conserved, exposed disulfide bridge (*Ct*EDEM Cys963-Cys985 and *Sc*Mnl1(Htm1) Cys712-Cys787);
2. mammalian EDEM3s (blue branch in Figure 1A): these proteins are the closest orthologues to unicellular EDEMs, featuring the linker region and the two C-terminal domains - but lack an obvious N-terminal membrane-associated region [50]. The PAD also contains the conserved, exposed disulfide bridge seen in the C-terminal domain of unicellular EDEMs (*Hs*EDEM3 Cys693-Cys714);
3. mammalian EDEM1s (isoform 2[2], orange branch in Figure 1A): the canonical EDEM1 isoform 2 lacks an N-terminal unstructured region [50], and has a ∼50 residue extension after the GH47 domain;
4. plant MNS5s (violet branch in Figure 1A): similar to mammalian EDEM1s but without any membrane-associated N-terminal helix;
5. mammalian EDEM2s (yellow branch in Figure 1A): they also feature a C-terminal extension following the GH47 domain;
6. plant MNS4s (green branch in Figure 1A): these proteins appear to be close to mammalian EDEM2s and have an N-terminal membrane-associated region [50].

   Sequence-based methods produce similar results, except that EDEM1s (orange branch in Figure 1B) are classified as evolutionarily closer to unicellular eukaryotic EDEMs than EDEM3s (blue branch in Figure 1B).

The stretch of EDEM1 sequence following the GH47 domain (IDR(C)) is disordered and interacts with the fourth thioredoxin-like domain (TRX4) of the partner PDI, ERdj5 [51, 52]. Sequence analysis identifies a similar region in EDEM2, EDEM3 and

[1]The Golgi endo-α-1,2-mannosidase (MANEA) which cleaves the A branch of the *N*-linked glycan belongs to a different fold family [42]

[2]The unstructured N-terminal region of the EDEM1 isoform 1 aligns well with the N-terminal section of fungal EDEMs - but the protein lacks the extra C-terminal domains. Structure-based and sequence-based phylogeny therefore give different results and EDEM isoform 1 sequences have been omitted from the structure-based analysis.

their orthologues. In unicellular EDEMs and EDEM3s the GH47 tail is longer (about ∼80 residues) and it is followed by one or two C-terminal domains. For this reason, the EDEM3 GH47 tail is often referred to as the linker region.

Oxidation of a conserved disulfide bond in the EDEM GH47 domain is necessary for function and requires PDI association

Structure-based sequence alignment [53] of the GH47 domain and linker region of unicellular EDEMs and mammalian EDEM3s, based on the available `AlphaFold` models [54] (Supplementary Figures S2 and S3) reveals that EDEMs share a conserved, surface-exposed intra-molecular disulfide, *e.g.* *Ct*EDEM C99-C558; *Hs*EDEM3 C82-C441; *Sc*Mnl1/Htm1 C65-C445; *Hs*EDEM1 C160-C529; *Hs*EDEM2 C65-C408 (Supplementary Figure S3). This disulfide bond is very close to the GH47 domain glycan binding site (see Figure 2C) and its oxidation is necessary for EDEM competency/function: after reduction of SS bonds by excess glutathione *in vitro*, EDEM3 enzymatic activity can be restored by its partner PDI ERp46, suggesting that this intramolecular SS bond is in mutual redox dependency with one of the PDI CXXC motifs and/or the intermolecular disulfide(s) mediating the covalent EDEM:PDI association [37]. Similar data suggest the same for *Sc*Mnl1/Htm1 and *Hs*EDEM2 [17, 25]. It is tempting to speculate that all ERAD mannosidases need SS-bond mediated association with their partner PDI and the oxidation of their intramolecular conserved SS bond to be active [17, 25, 37].

Unpaired Cys residue(s) in the EDEM GH47 tails

In all EDEMs, the GH47 tail contains a conserved Cys residue (termed Cys A), *e.g.* *Hs*EDEM1 Cys629 (*Mm*EDEM1 Cys624); *Hs*EDEM2 Cys558; *Hs*EDEM3 Cys528 (*Mm*EDEM3 Cys529); *Sc*Mnl1/Htm1 Cys579 and *Ct*EDEM Cys647. In yeast, Cys A can establish an EDEM:PDI intermolecular disulfide bond with the first Cys of one of the redox-active CXXC motifs on the PDI [25]. Indeed, in the *Sc*Mnl1/Htm1:*Sc*Pdi1 Cryo-EM structure, *Sc*Mnl1/Htm1 Cys579 is within disulfide bond distance from Cys406 of the ^{406}CXXC^{409} motif of the first TRX domain (TRX1) of *Sc*Pdi1 [28]. Homology modelling and biochemical data on the same proteins also suggest an equivalent inter-molecular disulfide bridge involving Cys A and one of the redox-active CXXC motifs on the PDI in each of the three human ERAD checkpoint EDEM:PDI complexes[3].

As already mentioned, the linker regions of unicellular EDEMs and EDEM3s are longer than the stretch following GH47 domains in EDEM1s and EDEM2s. In that linker, each of these sequences has a second unpaired cysteine residue termed Cys B, located downstream from Cys A and preceding the C-terminal domains (Supplementary Figure S3): *e.g.* *Sc*Mnl1/Htm1 C644, *Ct*EDEM C719, *Mm*EDEM3 C558, *Hs*EDEM3 C557 (Supplementary Figure S3). Biochemical data,

[3]In the *Hs*EDEM1:ERdj5 complex, Cys158 of the ^{158}CXXC^{161} motif in the first TRX domain (TRX1) of *Hs*ERdj5 can form a disulfide with *Hs*EDEM1 Cys629 [52]; in the *Hs*EDEM2:TXNDC11 complex, the disulfide bridge would be between Cys719 in the TRX2 domain of *Hs*TXNDC11 and *Hs*EDEM2 Cys558 [17, 35]; and in the EDEM3:ERp46 complex, between Cys217 in the TRX2 domain of *Hs*ERp46 [17] and *Hs*EDEM3 Cys528.

the *Sc*Mnl1/Htm1:*Sc*Pdi1 Cryo-EM structure and homology modelling suggest that Cys B in unicellular EDEMs and EDEM3s can also form an inter-molecular disulfide bond with the partner PDI [25, 28, 37].

The *Chaetomium thermophilum* EDEM:PDI heterodimer functions as an ERAD checkpoint in plants and human cells

Structural biology on eukaryotic proteins can profit from the enhanced protein stability of the thermophilic yeast *Chaetomium thermophilum (Ct)* [55]. A search in the *Ct* genome using the protein sequence of *Sc*Mnl1/Htm1 yields Uniprot entry https://www.uniprot.org/uniprot/G0SCX7 (hereinafter *Ct*EDEM), annotated as α-1,2-mannosidase; a search in the same genome using the protein sequence of *Sc*PDI1 yields Uniprot entry https://www.uniprot.org/uniprot/G0SGS2 (hereinafter *Ct*PDI), annotated as a protein disulfide isomerase. In agreement with the phylogenetic analysis, the same Uniprot entries were hit by searching the *Ct* genome with the sequences of *Hs*EDEM3 [32] and its partner PDI *Hs*ERp46 [37], respectively.

First, we set out to assay ERAD mannosidase activity of *Ct*EDEM. We did so *in planta*, using a complementation transfection assay in *Arabidopsis thaliana* (*A. thaliana*). The assay readout relies on the dwarf plant phenotype associated with expression of a mutant of the Brassinosteroid-Insensitive 1 (BRI1) growth receptor: the *bri1-5* mutant retains residual growth receptor activity but it is degraded by the plant EDEMs, called MNS4 and 5, which are ultimately responsible for the *bri1-5* plant dwarf phenotype. When MNS4 and MNS5 are deleted in the *bri1-5* background (triple mutant *At mns4-1 mns5-1 bri1-5*) the *bri1-5* receptor is not degraded, its secretion is restored and the associated residual activity is sufficient to rescue the WT growth phenotype [44, 56]. *Ct*EDEM transfection of the triple mutant *At mns4-1 mns5-1 bri1-5* resulted in functional re-complementation of EDEM, commitment of *bri1-5* to ERAD and restoration of the dwarf phenotype (Supplementary Figure S4). Use of fluorescent-tagged *Ct*EDEM constructs confirmed its localization to the plant ER (Supplementary Figure S5).

Secondly, we assayed *Ct*EDEM ERAD mannosidase activity in human cells. HEK293T EDEM3 KO cells were co-transfected with *Ct*EDEM, *Ct*PDI or both, together with a canonical ERAD substrate, the $\text{Null}_{\text{HongKong}}$ variant of α1-antitrypsin (A1AT-NHK, Supplementary Figures S4B, C and D). A1AT-NHK has been proven to be a substrate for both human EDEM1 [29] and human EDEM3 [32]. Following cleavage of the secretory signal peptide upon entry to the ER, A1AT retains a single cysteine residue (Cys 232) which can either form an inter-molecular disulfide bond with human ERAD checkpoint complexes, or with itself, leading to A1AT dimers and prolonged retention within the ER [57]. When *Ct*PDI was over-expressed in human cells in the absence of *Ct*EDEM the A1AT-NHK dimer:monomer equilibrium shifts towards the monomer (Supplementary Figure S4C). In human cells transfected with *Ct*EDEM (both alone and with *Ct*PDI) degradation of A1AT-NHK is enhanced, with reduction in both dimeric and monomeric protein levels (Supplementary Figures S4B and D).

The Cryo-EM structure of *Ct*EDEM:*Ct*PDI

The *Ct*EDEM:*Ct*PDI ERAD checkpoint complex was expressed and purified from HEK293F cells using affinity and size exclusion chromatography, and Cryo-EM grids were prepared with a *Ct*EDEM:*Ct*PDI sample eluted from a Micro-SEC column (Supplementary Figures S6 and S7). Cryo-EM data collection yielded a total of 11,208 micrographs (Supplementary Table S2) from which a total of 6,579,255 particles were picked and selected by rounds of 2D classification. After *ab initio* reconstruction and three rounds of decoy classification using cryoSPARC™ with heterogenous refinement, 3D classification on a subset of 624,939 particles gave four 3D classes for the complex. The largest volume pertains to a class with approximate dimensions 120x90x70 Å (Supplementary Figure S8A), which has strong density for all but the C-terminal domains of *Ct*EDEM. Initially, the GFP tag at the EDEM N-terminus had visible map density which was then removed by particle subtraction. The local resolution of this Cryo-EM reconstruction varies between 2.7 Å in the core of the GH47 *Ct*EDEM domain, to 2.8-3.2 Å in the four TRX domains of the *Ct*PDI to 3.8-5.5 Å in the C-terminal domains of *Ct*EDEM (Supplementary Figure S9).

`AlphaFold` domain models were initially docked into the Cryo-EM map by phased molecular replacement using `CCP4-Molrep` [58], followed by iterative model building and refinement. The EDEM catalytic domain nestles inside the curved arc formed by the PDI thioredoxin (TRX) domains TRX1, TRX3 and TRX4 (yellow, brick-red and red domains in Figures 2A and B). The exposed *Ct*EDEM Leu656 forms an intermolecular hydrophobic contact with the *Ct*PDI surface pocket formed by Tyr238, Tyr250 and His290, equivalently to what was observed in the *Sc*Mnl1/Htm1:*Sc*PDI1 orthologous complex structure, in which *Sc*Mnl1/Htm1 Trp592 and Tyr593 interact with *Sc*PDI1 Phe249, Tyr261 and His301 [28].

The first three TRX domains of *Ct*PDI adopt the threefoil/cloverleaf structure typical of the N-terminal portion of most PDIs (yellow, orange and brick-red domains at the top of Figures 2A and B), with TRX2 jutting out and not contacting *Ct*EDEM at all. The IMD and PAD [49] (*Ct*EDEM residues 726-821, 1069-1092 and residues 822-1068, respectively) project out from the GH47 domain (Figures 2A and B). *Ct*EDEM residues 1069-1083 following the PAD, contribute two β strands to the IMD β sandwich, *i.e.* the PAD is an insertion in the sequence encoding the IMD. The *Ct*EDEM N-terminal sequence 1-63, predicted to contain a trans-membrane helix [50], had been removed by cloning, and so was the ER retrieval C-terminal HDEL motif of *Ct*PDI. A 56-residue stretch of *Ct*EDEM PAD sequence (845-900) and the C-termini of both proteins (*Ct*EDEM 1084-1093 and *Ct*PDI 484-515) could not be traced. The final model analysed in `MolProbity` [59] has $\text{Rmsd}_{\text{bonds}}$= 0.016 Å and $\text{Rmsd}_{\text{bonds}}$= 0.9°; 7.2% (1249/1433) of all residues are in favored (98%) regions and 99.6% (1427/1433) of all residues were in allowed (>99.8%) regions in the Ramachandran plot.

The refined model and Cryo-EM map were deposited in the Protein Databank (PDB) and in the Electron Microscopy Data Bank (EMDB), with deposition IDs 8PKO and EMD-17749, respectively. Between the deposition of the structure and its release, *Ct*EDEM:*Ct*PDI was contributed to the list of CASP-15 protein prediction targets (CASP-15 Target H1157, https://predictioncenter.

org/casp15/target.cgi?id=116&view=all): a brief description of how the predictors did on this target was published in [60]. During the preparation of this manuscript, a paper describing the Cryo-EM structure of *Sc*Mnl1/Htm1:*Sc*PDI1 was published [28] and deposited (EMDB and PDB accession codes EMD-60365 and 8ZPW, respectively). The *Sc*Mnl1/Htm1:*Sc*PDI1 structure has equivalent quaternary structure to *Ct*EDEM:*Ct*PDI. The GH47 domains are very similar: overall *Sc*Mnl1/Htm1$_{GH47}$:*Ct*EDEM$_{GH47}$ rmsd$_{C\alpha}$ over 397 residues is 1.0 Å. The *Sc*PDI1:*Ct*PDI rmsd$_{C\alpha}$ over 402 residues is 3.2 Å.

The *Ct*EDEM mannosidase

As predicted by the `AlphaFold` model, the catalytic domain of the mannosidase (*Ct*EDEM residues 64-615) has the classic GH47 (α/α)7-barrel fold, with the active site at the base of the barrel, plugged by a β-hairpin at the C-terminus (*Ct*EDEM residues 602-615, Figures 2A and B) [61, 62]. The *Ct*EDEM active site features the canonical GH47 conserved acidic catalytic residues E191, D370, E522, and the conserved T608 coordinating the Ca^{++} ion with its main chain carbonyl and $O_{\gamma 1}$ atom (see Figures 2C and D and blue triangles in Supplementary Figure S3)[4].

In other deposited apo GH47 structures, the octahedral coordination of the catalytic divalent ion is usually completed by six water molecules [61, 62]. Substrate binding usually displaces two of the water molecules through coordination with the O2' and O3' hydroxyls of the terminal α1,2-mannose residue within the catalytic -1 subsite. In our Cryo-EM map there is density for a ligand bound in the active site, which was built as D-mannose with the coordination geometry observed in similar structures [5], see Figure 2C [41].

The GH47 domain is followed by a 120-AA long EDEM-specific portion of structure (*Ct*EDEM residues 616-725) which mediates most of the contacts to the PDI. The first stretch of this portion (*Ct*EDEM residues 616-651, coloured cyan in Figures 2A and B) is an L-shaped linker which starts after the GH47 C-terminal hairpin, sits over *Ct*EDEM helices α9/α10 and α13/α14 and wraps over the surface of the PDI TRX4 domain, eventually running parallel to the PDI TRX3-TRX4 linker (*Ct*PDI residues 616-655). This L-shaped linker contains the conserved *Ct*EDEM Cys647 that forms the inter-molecular SS bond to *Ct*PDI Cys385 of the PDI-TRX4 CXXC redox motif (the disulfide bond is labelled "SS1" in Figures 2A and B and its close-up view is shown in Supplementary Figure S10B). This disulfide bond is structurally and functionally equivalent to the one between EDEMs Cys A and their partner PDI, which is necessary for function, *e.g.* [17, 35].

After the L-shaped linker, a helical linker sub-domain (*Ct*EDEM residues 656-713, cyan in Figures 2A and B) nestles between helices α14/α15 of the GH47 domain and the TRX1 domain of the PDI. A `Dali` search [66] with the linker sub-domain does not

[4] *Ct*EDEM E191 is the residue corresponding to *Mm*EDEM3E147, *Hs*EDEM1 E225, *Mm*EDEM1 E220 and *Hs*EDEM2 E117 each of which when mutated to Q abrogate mannosidase activity respectively [16, 32, 63, 64]. *Ct*EDEM D370 is the residue corresponding to *Sc*Mnl1/Htm1 D279 which when mutated to N abrogates mannosidase activity [15]. *Ct*EDEM E522 is the residue corresponding to *At*MNS4 E376 and *At*MNS5 E388 which when mutated to N abrogate mannosidase activity [44].

[5] The ligand pose is similar to the one of D-Mannose analogues 1-deoxymannojirimycin and kifunensine (PDB IDs 1FO2 and 1FO3) [61] and of the -1 mannose ring of the thio-disaccharide substrate analogue co-crystallised in the active site of the GH47 domain of ER Man IB (PDB ID 5KK7 [65]).

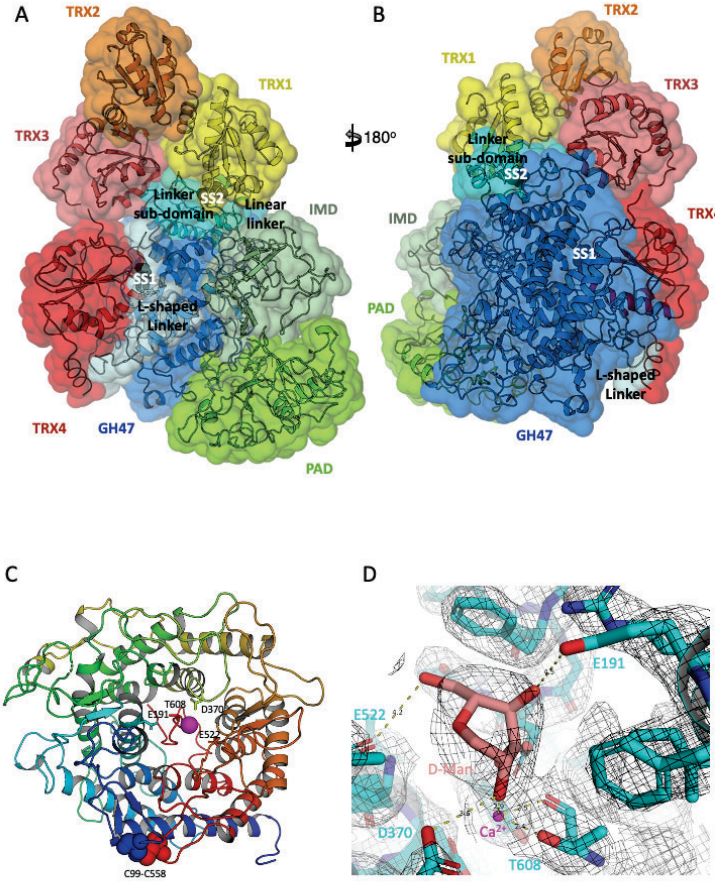

Fig. 2 The Cryo-EM *Ct*EDEM:*Ct*PDI ERAD checkpoint structure. A,B: Two views of the *Ct*EDEM:*Ct*PDI ERAD checkpoint structure in cartoon and transparent surface representation. Left-hand and right-hand side view are related by a rotation of 180 ° around the vertical axis. *Ct*EDEM domains: GH47 catalytic domain (56-615, blue); L-shaped linker, linker domain and linear linker (616-655, pale cyan; 656-713, cyan; and 714-725, green cyan); IMD (726-821 and 1069-1092, pale green); PAD (822-1068, green). *Ct*PDI domains: TRX1 (18-128, dark yellow); TRX2 (129-228, orange); TRX3 (229-342, brick red); TRX4 (343-484, red). The Ca^{++} ion is a magenta sphere. The two inter-chain disulfide bonds are represented in spheres and labelled SS1 (*Ct*EDEM Cys647:*Ct*PDI Cys385) and SS2 (*Ct*EDEM Cys719:*Ct*PDI Cys50); **C**: cartoon representation of the *Ct*EDEM GH47 catalytic domain, painted blue to red from N- to C-terminus. The side chains of the catalytic site conserved residues E191, D370, E522 and T608 are in sticks representation. The conserved *Ct*EDEM C99-C558 intramolecular disulfide bond is in spheres representation. **D**: Cryo-EM map in the *Ct*EDEM active site, represented as a mesh at level 10.0σ. O atoms: red; N atoms: blue; protein C atoms: cyan; D-mannose C atoms: salmon. The distances between the D-mannose/Ca^{++} ion and their coordinating residues are represented as dashed yellow lines. Figure made in `PyMOL`.

detect any structural homology with any of the protein domains in the Protein Databank. This sub-domain is followed by a short linear linkage motif (*Ct*EDEM residues 714-725) which contains the conserved *Ct*EDEM Cys719 forming the inter-molecular SS bond to *Ct*PDI Cys50 of the PDI-TRX1 CXXC redox motif. This disulfide bond is labelled "SS2" in Figures 2A and B and a close-up view shown in Figure S10A. This disulfide bond is structurally and functionally equivalent to the one hypothesised between EDEMs Cys B and their partner PDI [25, 28, 37].

As already mentioned, the IMD and PAD are topologically intertwined (Figure 2C). The PAD is encoded by a stretch of sequence between the majority of the IMD and the C-terminal 24 residues of the *Ct*EDEM protein. The latter form a two-stranded β sheet that completes the β sandwich fold of the IMD. `AlphaFold` correctly predicted this topological feature but did not predict correctly the relative orientation of the IMD-PAD tandem with respect to the GH47 domain. The main IMD:GH47 contact is formed by the hairpin *Ct*EDEM residues 778-782 (Figure 2C), nestling in a shallow surface pocket of the GH47 domain (*Ct*EDEM residues 437-460).

The observed *Ct*EDEM:*Ct*PDI interface rationalises the loss of function of mutants of *Ct*EDEM orthologues. *Sc*Mnl1/Htm1 mutants D607A, E627A, W636A, F632L and Y633S abrogate the association with *Sc*PDI1 [25, 67]; the G343E mutant of the *Arabidopsis thaliana* plant EDEM orthologue MNS5 abrogates ERAD mannosidase function. The equivalent residues in *Ct*EDEM R672, H669, L712, L703, Y704 and G477 respectively, all map to the interface between *Ct*EDEM and *Ct*PDI in our structure (Supplementary Figure S11). The loss of function associated with the deletion of the 4 C-terminal residues of *Sc*Mnl1/Htm1 [25] is also explained by the damage inflicted to the fold of the IMD domain.

*Ct*EDEM glycan-specificity is associated with alterations at the entrance of the mannosidase active site

In mammals, there are seven GH47 members, including ER α1,2-mannosidase I (ERManI); the three Golgi α1,2-mannosidases GMIA, GMIB, and GMIC [65]; and the three ER degradation-enhancing α-mannosidase-like (EDEM) proteins (EDEM1 [16, 29, 52, 68, 69], EDEM2 [70], and EDEM3 [32]), the ERAD misfolded glycoprotein checkpoints. The GH47 domains of these proteins share a common fold and differ in insertion loops. Five *Ct*EDEM regions (labelled "II" to "VI", residues 140-150, 165-180, 205-235, 280-300, and 390-420 respectively) are surface loop insertions only present in thermophilic EDEMs but not in other GH47 domains (Supplementary Figures S3 and S12). These regions are contiguous in space and form a surface which is specific to thermophilic EDEMs but not to other orthologues (Supplementary Figure 3).

Structures of GH47 α1,2-mannosidases have been determined in the absence and presence of inhibitors, substrate analogues and substrate glycans [61, 62, 65, 71]. In contrast to the highly conserved -1 and +1 subsites, the structures of the substrate-binding groove are distinct among the GH47 family members. These groove features are the main determinants for selectivity towards the cognate *N*-linked glycan branch that inserts in the active site [65, 71].

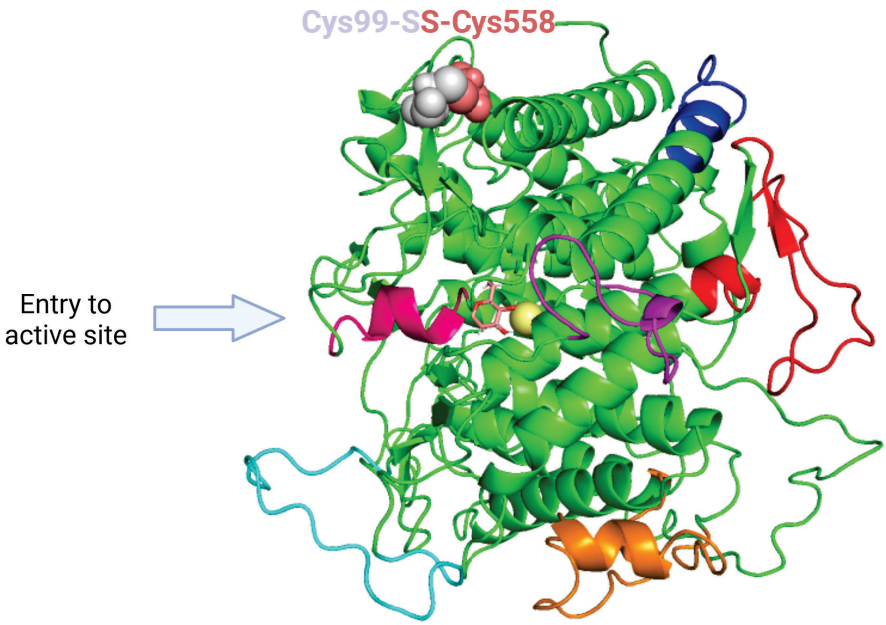

Fig. 3 *Ct*EDEM active site with short helix and loop insertions. Top view of the GH47 catalytic domain of *Ct*EDEM with short α helix and surface loop insertions highlighted. The short α helix, residues *Ct*EDEM 110-118 is highlighted in hot pink, the loop insertions of residues *Ct*EDEM 140-150, 165-180, 205-235, 280-300, and 390-420 are coloured dark blue, magenta, red, cyan, and orange respectively. These six regions correspond to I-VI in Figure S12. The Ca^{++} ion is represented as a sphere and coloured light yellow. The D-Mannose in the active site is coloured by atom (carbon = orange, oxygen = red). The conserved intramolecular disulfide bond is shown with Cys99 in light grey and Cys558 in salmon.

Region "I", *Ct*EDEM comprises residues 100-118 and is conserved across 600 or so *Ct*EDEM close orthologues (Supplementary Figure S12). In the structure, this region is a surface loop including an α helix (*Ct*EDEM helix α2, residues 111-118, Figure 3, hot pink) which is not present in the structures of ER Man IB and occupies the space where the first branching mannose of the N-glycan ("C" in Supplementary Figure S1) and the first mannose of the *N*-glycan A branch ("D" in Supplementary Figure S1) bind ER Man IB (PDB ID 5KIJ [65]) and Golgi α-Mannosidase IA (PDB ID 1DL2 [61]). The volume taken up by the *Ct*EDEM α helix in region "I" suggests that EDEMs bind the A branch of the *N*-linked glycan differently from ER Man IB and Golgi Man IA. In particular, at the position corresponding to *Ct*EDEM Val117, a methyl group is likely to be involved in contacting the "J" mannose in branch C (Supplementary Figure S1). This region's conformation depends on the formation of the conserved intramolecular disulfide bond, which only forms in presence of the partner PDI [17, 25, 37].

In the Cryo-EM map, *Ct*EDEM Cys303 appears modified covalently and was tentatively modelled as Cys-S-sulfonate [72] (this position is Thr or Ser in ER Man IB and Golgi α-Mannosidase IA, respectively). A key Arg residue (Arg273), conserved among the ER mannosidase IB subfamily of enzymes, was found to interact with several residues in their active site and to contribute to branch specificity [73]. The equivalent residue to Arg273 of ER Man1B in *Ct*EDEM is Gly368: in all EDEMs this residue is either Glycine or Serine (Supplementary Figure S3). As these are both smaller amino acids than Arg, this position may be a key determinant of glycan branch specificity in EDEMs vs. ER Man IB.

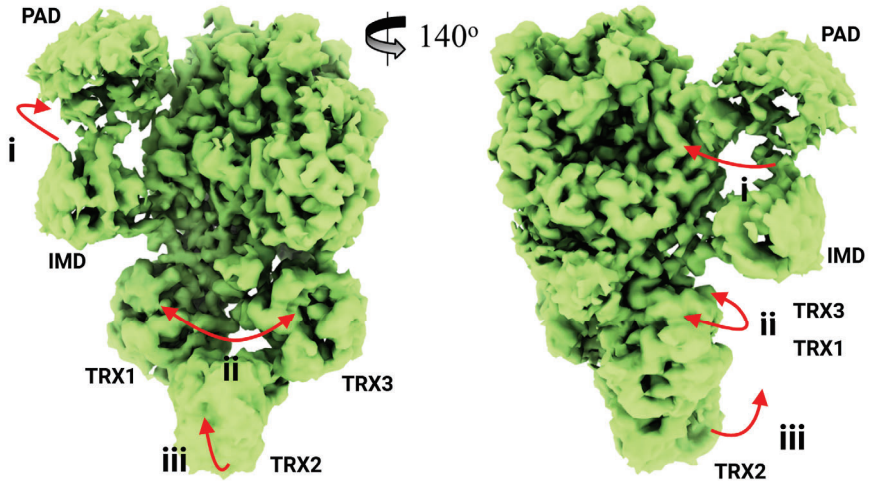

Fig. 4 *Ct*EDEM IMD-PAD and *Ct*PDI TRX1,2,3 domains exhibit a range of inter-domain conformations. 3D variability analysis in cryoSPARC displayed three principles ranges of motion: i) front-to-back and up-and-down action of the *Ct*EDEM IMD and PAD. ii) twisting movement of *Ct*PDI TRX1-3 domains. iii) flapping of the *Ct*PDI TRX2 domain.

*Ct*EDEM:*Ct*PDI inter-domain conformational flexibility

3D variability analysis (3DVA) in cryoSPARC™ was utilised to investigate the flexibility of *Ct*EDEM:*Ct*PDI portions built in volumes with lower local resolution. 3DVA analysis of the particles within the dataset suggested three specific motions. The first involves the IMD and PAD (Figure 4i) and the second and third involves the three-leaf clover PDI tail (Figure 4ii and 4iii). The first motion can be described as a twisting and pivoting of the IMD and PAD around the main axis of the particle and away from the active site face of the GH47 domain while the three-leaf clover and the GH47 domain remain relatively unperturbed (Supplementary Videos 1 and 2). The second and third motions involves a twisting of the TRX1-3 domains with respect to TRX4 and EDEM (Supplementary Video 4). Figure S13 shows EM maps obtained from particles sampling the endpoints of the third movement. The PDI three-leaf clover

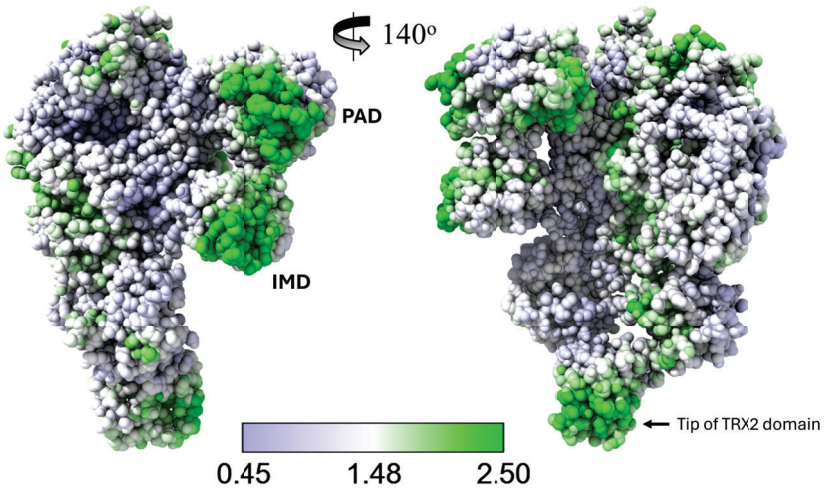

Fig. 5 *Ct*EDEM:*Ct*PDI surface hydrophobic patches localise to the flexible IMD-PAD and TRX2 domains. Two views (related by a rotation of 140° around the vertical axis) of the *Ct*EDEM:*Ct*PDI heterodimer model are displayed in spheres representation and coloured by surface hydrophobicity, calculated as the ratio of non-polar to polar residues [87]. Hydrophilic regions are painted pale violet and hydrophobic regions are painted green, as indicated by the hydrophobicity scale bar.

straightens (bends) with respect to the main body of the complex, so that the particle toggles between a linear (Figure S13A-C, yellow map) and a bent conformation (Figure S13A-C, blue map). Supplementary Video 3, shows the three-leaf clover undergoing an angular change of approximately 15°. The observed conformational flexibility is highly consistent with biophysical studies of PDIs [74, 75].

*Ct*EDEM:*Ct*PDI surface hydrophobic patches localise to the flexible IMD-PAD and TRX2 domains

The canonical function of the EDEM:PDI complex is to act as a checkpoint for ERAD, but the presence of the PDI is reminescent of the role of TRX domains in chaperone-promoted refolding [76, 77]. Chaperones often interact with exposed hydrophobic regions of misfolded proteins, limiting the risk of pathogenic aggregation and lowering energetic barriers to refolding pathways [78–80]. UGGT, the ER retention checkpoint, recognizes misfolded glycoproteins and delays ERAD targeting by substrate re-glucosylation [81]. In addition, UGGT may act as a re-folding chaperone [82, 83], forms a tight complex with the Sep15 thioredoxin [84], and its activity may be mediated by the ability of its thioredoxin-like (TRXL) domains to bind linear peptides [85, 86]. Inspired by the similarities between the UGGT:Sep15 ER retention checkpoint and the EDEM:PDI ERAD checkpoint, we set out to look for surface regions of the EDEM:PDI heterodimer with the potential to interact with exposed hydrophobic motifs of misfolded proteins. Non-polar surfaces were identified using the `protein-sol` server (https://protein-sol.manchester.ac.uk/) [87].

Two hydrophobic regions were identified on the EDEM:PDI surface: the face of the *Ct*EDEM IMD-PAD arm to the side of the GH47 face at the centre of which the active site is found (*Ct*EDEM IMD residues 728-732, 745-749, 792-794; PAD residues 832-835, 906-912, 939-947); and the lower tip of the *Ct*PDI TRX2 domain (*Ct*PDI, Val133, Leu138, Val150 and Phe141). These regions are coloured green in Figure 5. The same IMD-PAD and TRX2 domains have been identified as highly flexible (previous section), making them prime candidates as mediators of recruitment of misfolded glycoprotein substrates to the enzyme.

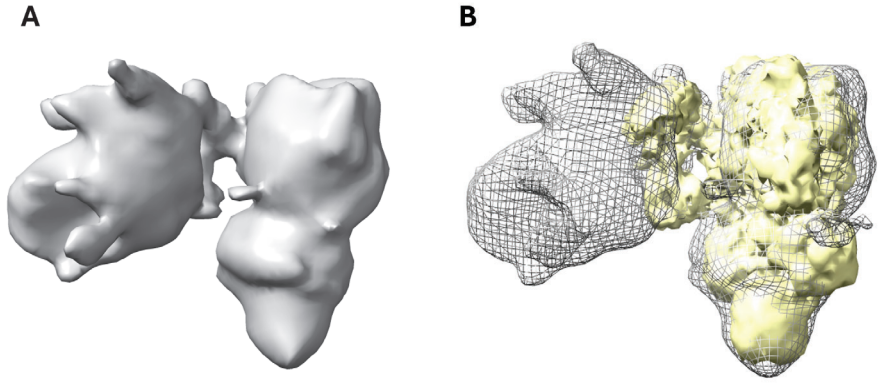

Fig. 6 Cryo-EM map of *Ct*EDEM:*Ct*PDI:A1AT-NHK with fitted *Ct*EDEM:*Ct*PDI heterodimer map A: The Cryo-EM map of *Ct*EDEM:*Ct*PDI:A1AT-NHK displayed in UCSF `ChimeraX` [88]. **B**: The map of *Ct*EDEM:*Ct*PDI:A1AT-NHK in grey mesh with the one of the *Ct*EDEM:*Ct*PDI heterodimer map fitted within and displayed as a yellow solid surface.

EDEM:PDI substrate recognition and recruitment

Having determined the structure of the *Ct* ERAD checkpoint complex, we next investigated its functional interactions with misfolded client proteins. Additionally, to probe the broader spectrum of client interactions, we employed biochemical assays and western blotting, using both *Ct*EDEM:*Ct*PDI and its human orthologous complex, *Hs*EDEM3:*Hs*Erp46. These complementary approaches provide mechanistic insights into substrate recognition and recruitment on the part of theERAD misfolding glycoprotein checkpoint complex.

*Ct*EDEM:*Ct*PDI interacts with NHK-A1AT substrate through the mobile C-terminal domains

Co-expression of *Ct*EDEM and *Ct*PDI in HEK293F cells was repeated adding a third plasmid encoding A1AT-NHK. A ternary complex of the three proteins (*Ct*EDEM:*Ct*PDI:A1AT-NHK) was purified (Supplementary Figure S14) and studied by cryo-EM. A dataset of 7773 movies was collected and processed similarly to what

described for the *Ct*EDEM:*Ct*PDI apo structure (Supplementary Figure S15). Two distinct populations of 2D classes were noticed, consistent with the heterodimer with or without A1AT-NHK. Initial reconstructions of the ternary complex particles were relatively low resolution but displayed clear density adjacent to the core heterodimer particle. A mask was generated to cover the heterodimer particle and used in a focused 3D classification. Four classes were generated and the best map and particles were taken forward for 3D refinement. The final *Ct*EDEM:*Ct*PDI:A1AT-NHK Cryo-EM map has an estimated global resolution of 9 Å although the region of extra density has lower local resolution, consistent with high conformational disorder (Figure 6A).

Overlaying the EM map of the *Ct*EDEM:*Ct*PDI heterodimer onto the ternary complex map shows a close fit (Figure 6B). The density for the bound A1AT-NHK substrate is visible adjacent to the *Ct*EDEM C-terminal domains in the heterodimer. No gross change in the relative orientations of EDEM and PDI is apparent at this resolution. The interface between A1AT-NHK and *Ct*EDEM:*Ct*PDI localises to the mobile *Ct*EDEM IMD-PAD arm. Mass spectrometry analysis of the same protein sample, detects the conserved intramolecular PAD disulfide *Ct*EDEM Cys963:Cys985 (Supplementary Figure S17A), A1AT-NHK disulfide bonded dimers (Supplementary Figure S17B), and an inter-molecular disulfide bond between the *Ct*EDEM Cys985 in the PAD and the A1AT-NHK client (Supplementary Figure S17C).

*Ct*EDEM:*Ct*PDI forms mixed disulfide bonds with A1AT-NHK

When a member of the PDI family acts as a foldase in the ER, the first cysteine in one of its CXXC redox motifs (*e.g.* **C**GHC in *Ct*PDI) can form an inter-molecular disulfide bond with an equivalent Cys residue in a second PDI copy, or a Cys residue in a PDI client protein [89], to facilitate re-folding of the same client via disulfide redox chemistry and/or SS bond isomerisation [90, 91]. Once the PDI client needs releasing, the second C-terminal cysteine in the CXXC motif re-forms a disulfide bond with the first, so that the PDI client and and its client are no longer covalently bound. However, if the CXXC C-terminal cysteine is mutated to a redox-inactive residue with similar chemical and steric properties (*e.g.* alanine or serine) the PDI and its client remain trapped by the disulfide bond. CXXA/S mutants of PDI family members are therefore known as trapping mutants [92].

Evidence that *Hs*ERp46 (the human EDEM3 partner) forms a mixed disulfide bond with a client glycoprotein has been obtained in the context of its refolding role, where it catalyses the reduction of non-native disulfides [93] but the role of *Hs*ERp46 mixed disulfides to ERAD clients has not been investigated. In order to test the hypothesis that *Hs*ERp46 may recruit a glycoprotein client to EDEM3 via mixed disulfide bonding, HEK293F cells were co-transfected with *Ct*EDEM, A1AT-NHK and either wild-type *Ct*PDI or the *Ct*PDI Cys53Ser trapping mutant. *Ct*EDEM:*Ct*PDI heterodimers and *Ct*EDEM:*Ct*PDI:A1AT-NHK ternary complexes were purified from the media by IMAC followed by SEC (Supplementary Figures S14 and S16).

The non-reducing Western blots of cells transfected with *Ct*EDEM, A1AT-NHK and the *Ct*PDI Cys53Ser trapping mutant detect *Ct*PDI and A1AT-NHK belonging to species of higher molecular weight than the *Ct*EDEM:*Ct*PDI heterodimer (middle strips in Figures 7A and B). The anti-A1AT-NHK Western blot of the same

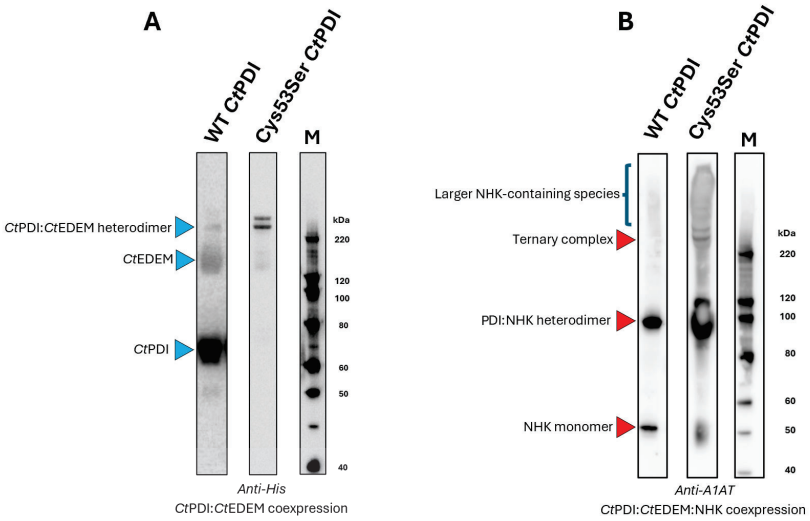

Fig. 7 Cys53Ser *Ct*PDI trapping mutant favours disulfide bond formation with *Ct*EDEM and A1AT-NHK. HEK293F cells were co-transfected with *Ct*EDEM A1AT-NHK and either wild-type *Ct*PDI or *Ct*PDI Cys53Ser trapping mutant. Heterodimer or Ternary complexes were purified from the media by IMAC followed by SEC (see Section on Protein purification). Fractions collections from both SEC experiments were loaded in non-reduced (NR) conditions in 4-12% polyacrylamide gels, transferred on nitrocellulose membrane and probed with indicated antibodies: rabbit anti-α1 Antitrypsin (A1AT), mouse anti-His for detection of *Ct*PDI and *Ct*EDEM. **A**: Anti-His Western blot from *Ct*EDEM:*Ct*PDI (WT and mutant) heterodimer co-purification with a SEC fraction corresponding to the heterodimer peak. **B**: Anti-A1AT Western blot from ternary complex co-purification with a SEC fraction corresponding to the ternary complex peak. The identity of the 100 kDa band as *Ct*PDI:NHK heterodimer was confirmed by Western blot with anti-His. Full purification SDS-PAGE and Western blot results are shown in Supplementary figures S14 and S16.

samples (Figure 7B) reveals that the *Ct*PDI Cys53Ser trapping mutant originates a variety of high molecular weight protein complexes that contain A1AT-NHK, while the monomeric A1AT-NHK band weakens: *Ct*EDEM:*Ct*PDI appears to disulfide bond to A1AT-NHK. *Ct*PDI is also detected bound to monomeric A1AT-NHK: the trapping mutant increases the amount of *Ct*EDEM:*Ct*PDI complex, consistent with the *Ct*EDEM Cys719-SS-*Ct*PDI Cys50 disulfide observed in the Cryo-EM structure, and suggesting reversible disulfide redox chemistry at the EDEM CysB intermolecular disulfide bond (left-hand side and middle strips in Figure 7B).

Mammalian EDEM3 function depend on intra- and inter-molecular redox chemistry

To gain insight into the role of redox chemistry in the EDEM3:ERp46 heterodimer, we generated EDEM3 and ERp46 Cys mutants. In EDEM, the single mutants *Mm*EDEM3 C529S and C558S abrogate the EDEM linker Cys A and Cys B, respectively; the double mutant C529S/C558S has no free Cys in the EDEM linker. In human ERp46, we generated the triple trapping mutant CXXA, *aka* “CA” - *Hs*ERp46

C92A/C220A/C353A - altering the resolving Cys of each of its TRX domains CXXC redox motifs: *Hs*ERp46 ^{89}CGHC^{92}, ^{217}CGHC^{220} and ^{350}CGHC^{353}. To probe the oxidation state of the EDEM, single and double Cys-to-Ser mutants that impair EDEM intramolecular disulfide bridge formation were also studied: *Mm*EDEM3 C83S, C442S and C83S/C442S. These mutants cannot form the EDEM intramolecular disulfide bond [52] so that only the reduced EDEM3 band is visibile in SDS-PAGE (lower band of the *Mm*EDEM3 doublet around 120 kDa in lanes 5-10 in Figure 8A).

Cys A in the EDEM3 linker region forms a stable disulfide to ERp46 and plays a role in EDEM3 oxidation

We studied *Mm*EDEM3:*Hs*ERp46 disulfide-bonded heterodimer formation by analysing the EDEM3 linker Cys mutants on non-reducing SDS-PAGE (lanes 11-16 in Figure 8A). In presence of WT ERp46, the strongest band for the oxidised *Mm*EDEM3:*Hs*ERp46 disulfide-bonded heterodimer was formed by *Mm*EDEM3 WT and its C558S mutant (Figure 8A, upper band of the doublet around 200 kDa in lanes 3 and 13). The *Mm*EDEM3 C5529S (no Cys A in linker) and *Mm*EDEM3 C529S/C558S (no free Cys in linker) mutants cause an increase in the amounts of the reduced form of EDEM3 (lower band of the doublet around 120 kDa in Figure 8A, lanes 11, 12, 15 and 16). Together, these observations suggest that intermolecular disulfide redox chemistry following the establishment of an intermolecular disulfide between a Cys residues in ERp46 and EDEM3 Cys A (*Mm*EDEM3 C529) enhances EDEM3 oxidation. This observation is in keeping with the homology models of mammalian EDEM3:ERp46 complexes, in which the EDEM3 linker Cys A (*i.e.* *Hs*EDEM3 C528 or *Mm*EDEM3 C529) is disulfide linked to C217 in the *Hs*ERp46 ^{217}CXXC^{220} redox motif.

In an assay of mannose-trimming activity, no mannosidase activity was detected for the *Mm*EDEM3 C529S and C529S/C558S mutants up to 6 h of incubation (Figure 8C, lanes 3, 5, 8, 10, 13, and 15). Only after 24 h of incubation mild mannose-trimming activity was observed (Figure 8C, lanes 18 and 20), consistent with equivalent observations for the Cys A mutant of *Sc*Htm1p/Mnl1p in the *Sc* heterodimer [28]. Either ERp46-independent EDEM3 slow oxidation can take place or EDEM3C529S and C529/558S mutants can weakly associate with ERp46 independently of C529.

The *Hs*ERp46 ^{217}CXXC^{220} motif is required for establishment of the intermolecular disulfide to EDEM3 Cys A

Interestingly, the *Mm*EDEM3:*Hs*ERp46 heterodimer doublet band is absent from the samples co-transfected with *Mm*EDEM3 WT (or C558S) and the ERp46 CXXA triple trapping mutant (Figure 8A, lanes 4 and 14), even if these EDEM3 mutants have an intact Cys A: enhanced laddering is also observed at molecular weights $\geq$ 250 kDa. To probe which of the three trapping mutants most affects the formation of the disulfide bridge with *Mm*EDEM3 Cys A, we studied the *Hs*ERp46 C92A, C220A and C353A single trapping mutants, as well as the double trapping mutant C92A/C353A. All the *Hs*ERp46 trapping mutants apart from CXXA and C220A formed the *Mm*EDEM3:HsERp46 disulfide-bonded heterodimer (Figure 8B, lanes 5-7). The C220A mutation causes the usual heterodimer band around 150 kDa to disappear

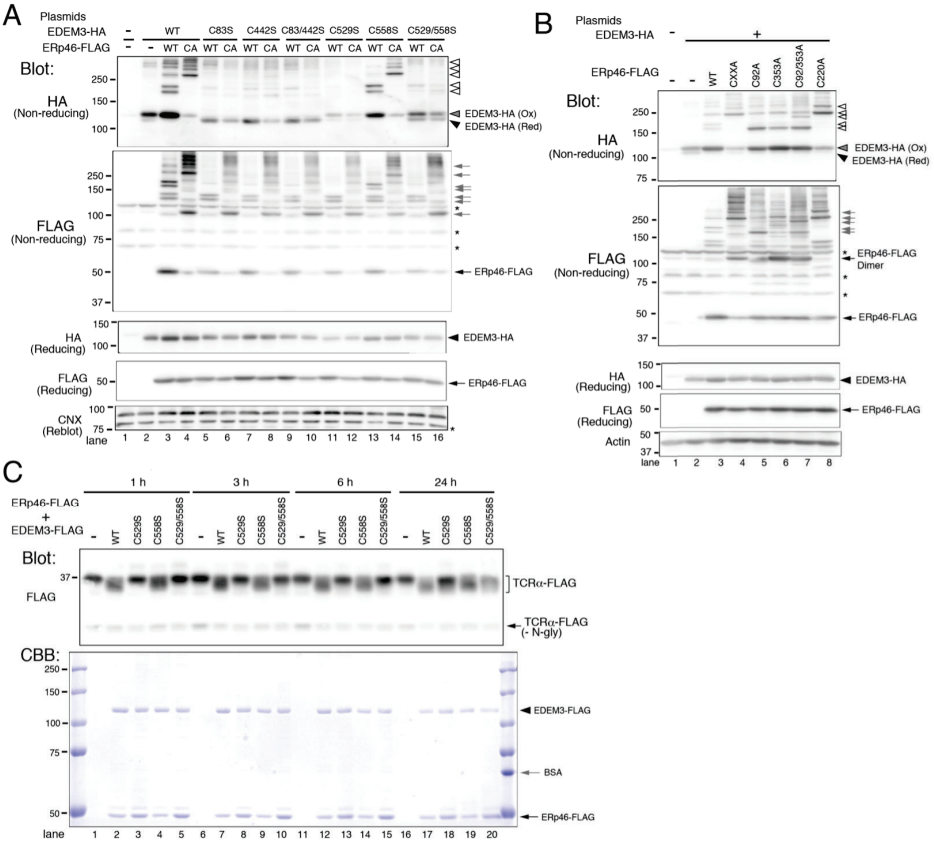

Fig. 8 Mammalian EDEM3:ERp46 disulfide bonds and activity assay. HEK293 were transfected with *Mm*EDEM3-HA and *Hs*ERp46-FLAG and cell lysates were separated by SDS-PAGE under reducing or non-reducing conditions. Disulfide-bonded complexes were analyzed by Western blotting (A, B), and mannosidase activity was assessed *in vitro* using TCRα-FLAG as a substrate (C). Black filled triangles indicate reduced *Mm*EDEM3-HA and gray filled triangles shows oxidized *Mm*EDEM3-HA. Open white triangles indicate disulfide-bonded high molecular weight complexes containing *Mm*EDEM3-HA. Black arrows indicate ERp46-FLAG monomer, and gray arrows denote disulfide-bonded high molecular weight complexes containing ERp46-FLAG. Asterisks indicate non-specific signals detected by the antibodies. **A:** *Mm*EDEM3 (WT or a Cys-to-Ser mutant) was co-expressed with ERp46-FLAG (WT or the triple trapping mutant CXXA, *aka* "CA": *Hs*ERp46 C92A/C220A/C353A). **B:** Cells were co-transfected with WT *Mm*EDEM3-HA and a *Hs*ERp46 single, double or triple trapping mutant, as indicated. **C:** EDEM activity *in vitro* was analyzed using TCRα-FLAG as a substrate. HEK293 cells were co-transfected with *Mm*EDEM3-HA (WT or a Cys-to-Ser mutant) and WT *Hs*ERp46-FLAG. The heterodimer was purified, incubated with TCRα-FLAG at 37°C for the indicated period. Top panel: EDEM activity was detected by the Western blotting, following the loss of mannose by the size-shift of the$\sim$37 kDa TCRα-FLAG band on the gel. The non-glycosylated TCRα-FLAG is visible as a faint band labelled (- *N*-gly). Bottom panel: the upper part of the gel was stained with Coomassie Brilliant Blue, with 1 μg of Bovine Serum Albumin (BSA) loaded in the last lane together with Molecular Weight Markers, in order to estimate the amount of purified proteins.

(Figure 8B, lanes 4 and 8) and higher MW bands intensify. This is reminescent of the disappearance of the *Mm*EDEM3:HsERp46 heterodimer band in *Mm*EDEM3 mutants lacking Cys A (C529, data not shown).

Equivalent results were obtained with EDEM3 KO HEK293T cells co-transfected with *Hs*EDEM3 and *Hs*ERp46 WT and trapping mutants (Supplementary Figure S18). Introduction of the C220A trapping mutation in *Hs*ERp46 resulted in disappearance of the species corresponding to the disulfide-bonded *Hs*EDEM3:*Hs*ERp46 heterodimer in a Western blot of the gel using an anti-EDEM3 antibody (lanes labelled CXXA and C220A in Supplementary Figure S18A). Enhanced laddering is also observed at higher MWs in CXXA and C220A. A mass shift upwards of the heterodimer species is not visible on the gel when blotting with an anti-ERp46-flag antibody (Supplementary Figure S18B), likely because of the negligible amounts of ERp46 trapping mutants bound to clients in the context of the ERAD glycoprotein misfolding complex, the majority of the ERp46 trapping mutant likely bound to folding glycoproteins in its capacity of disulfide isomerase [93].

Discussion

The ERAD checkpoint complex is essential for safeguarding eukaryotic cells against the accumulation of misfolded glycoproteins, glycoproteins themselves constitute about a third of the proteome [94]. Our study provides the most comprehensive structural and mechanistic insights to date into the function of the ERAD checkpoint complex, integrating cryo-EM structural studies, phylogenetic analyses, and biochemical data.

Cryo-EM structures of the ERAD checkpoint complex in both apo and ternary states (EDEM:PDI:A1AT-NHK) reveal two primary mechanisms for substrate recognition. The first involves recruitment of misfolded glycoproteins through solvent-exposed hydrophobic regions, aligning with prior observations that EDEM's flexible IMD-PAD domain dynamically engages unfolded substrates. The second mechanism is mediated by reversible disulfide bonding between PDI and the substrate, allowing recognition of aberrant disulfide-linked multimers.

Phylogenetic and sequence analyses identify conserved disulfide-linked regulatory elements across eukaryotic EDEMs, from early eukaryotes to humans. The conserved intramolecular disulfide bond in the catalytic domain of all EDEMs, as well as unpaired cysteine residues at the C-terminal end of the catalytic domain, play critical roles in substrate processing. Notably, unicellular EDEMs and mammalian EDEM3s possess an additional unpaired cysteine that may further tighten the EDEM:PDI interaction and/or be involved in redox chemistry and/or SSbond isomerism with clients.

Our findings also provide new insights into how the ERAD checkpoint selects glycoproteins for degradation. A short α-helix at the EDEM active site entry restricts access, ensuring specificity for mannose cleavage from Branch C, a key determinant in terminal misfolding signals. This specificity aligns with prior observations of glycan processing requirements in ERAD [64, 95]. However, glycan binding alone is not required for EDEM:PDI-mediated substrate recognition, as evidenced by interactions

with NHK-A1AT even in the presence of kifunensine, which inhibits substrate binding. Instead, exposed hydrophobic surfaces and aberrant cysteine pairing likely serve as critical misfold recognition features.

The *Ct*EDEM:*Ct*PDI:A1AT-NHK structure provides strong support for the hypothesis that the PAD recruits misfolded substrates *in situ* analogous to recruitment in chaperones, similarly to what was suggested for the C-terminal domain of *Sc*Mnl1/Htm1 [28]. The volume corresponding to the A1AT-NHK substrate is larger than expected for a single copy of A1AT-NHK. This could be because of inherent inter-domain mobility of the substrate relative to the checkpoint core, but a corresponding reduction in its average density is not observed. Alternatively A1AT-NHK may bind this site in dimeric and/or oligomeric states.

The non-reducing Western blots of protein purified from cells transfected with *Ct*EDEM A1AT-NHK and the *Ct*PDI Cys53Ser trapping mutant suggest that PDI Cys50 (*Ct*PDI Cys B) can bind either a Cys in *Ct*EDEM or a Cys in the client. By the latter covalent link to a glycosylated client the PDI may increases the avidity of the EDEM catalytic site for (one of) the client's N-linked glycan to be de-mannosylated [96].

Lack of the *Mm*EDEM3:*Hs*ERp46 and *Hs*EDEM3:*Hs*ERp46 heterodimer bands in non-reducing SDS-PAGE gels when *Hs*ERp46 Cys220 is mutated is in keeping with mammalian EDEM3:ERp46 homology models, which show a disulfide bond between EDEM3 Cys A and the first Cys of the ^{217}CGHC^{220} CXXC motif, *Hs*ERp46 Cys217. In absence of externally supplied oxidising equivalents, establishment of an intermolecular disulfide between an EDEM free Cys and the first Cys of an ERp46 CXXC motif takes place via disulfide bond isomerism: in this scenario, formation of the EDEM3 Cys A disulfide bond with *Hs*ERp46 Cys217 requires an intact *Hs*ERp46 ^{217}CXXC^{220} motif. The enhanced high-molecular weight laddering observed whenever Cys220 is mutated is also compatible with an increase in disulfide-bridged ERp46-SS-client complexes: a Cys220 trapping mutant may sequester the majority of *Hs*ERp46 Cys217 in a mixed disulfide with a client, so that the EDEM3:ERp46 heterodimer cannot form.

Last but not least, published observations, re-interpreted in the light of our data, suggest that the EDEM GH47 domain is misfolded in isolation within the ER due to a reduced conserved intramolecular disulfide bond [25, 97]. Association with the PDI leads to an active EDEM:PDI complex, where the EDEM GH47 domain folds into a competent mannosidase while the PDI CXXC motif is reduced. This redox exchange enables EDEM to perform demannosylation — signaling terminal misfolding — while the PDI can function as an ERAD reductase, facilitating retro-translocation of misfolded glycoproteins [34, 98–100]. As to the source of the oxidising equivalents to be transferred to the EDEM intramolecular disulfide, it is interesting to notice that using the first Cys of its ^{217}CXXC^{220} redox motif, *Hs*ERp46 can form intermolecular disulfide bonds with peroxiredoxin 4 (PRXD4) [101, 102]. This raises the possibility that PRXD4, oxidized during the reduction of hydrogen peroxide to water, transfers its disulfide bond to ERp46 through a thiol-disulfide exchange, oxidizing the ERp46 Cys217–Cys220 motif. A mixed disulfide with EDEM3 Cys A-SS-ERp46 Cys217 can then form by disulfide isomerism, and this intermolecular disulfide in turn can oxidise the EDEM3 intramolecular disulfide, releasing reduced ERp46. The reduced ERp46

can be reoxidized by PRXD4, completing a catalytic cycle where the oxidizing equivalents originated from Prx4 are relayed through ERp46 to drive EDEM3 intramolecular disulfide bond formation.

Beyond ERAD substrate processing in general, our findings have implications for protein misfolding disorders such as α1-antitrypsin deficiency (A1ATD) [5, 103]. The misfolded A1AT-Z variant, responsible for the most severe forms of A1ATD [104, 105], is primarily targeted by ERAD. Our structural data indicate that disrupting misfold interactions — either by modifying hydrophobic engagement or interfering with disulfide bond formation — could provide therapeutic strategies to mitigate the loss-of-function effects associated with A1ATD [106–109].

Together, our results clarify key mechanistic roles of the EDEM:PDI checkpoint complex in ERAD and set the foundation for targeting these interactions in protein misfolding diseases. By linking structural insights with functional validation, we provide a framework for future therapeutic strategies aimed at modulating ERAD activity in disease contexts.

Methods

Phylogeny

Sequence sets were constructed starting from the `AlphaFold Clusters` repository (https://cluster.foldseek.com/, [48]) in order to profit from the curation criteria used to label the entries (including ≥50% identity and ≥90% overlap in sequence length) and from easy identification of the cluster members by UniProt IDs (*e.g. Homo sapiens* EDEM1:Q92611, EDEM2:Q9BV94, EDEM3:Q9BZQ6; *Arabidopsis thaliana* MNS4:Q9FG93, MNS5:Q9SXC9; *Chaetomium thermophilum* EDEM: G0SCX7).

The phylogenetic analysis was carried out with `IQ-TREE 2` [110] and the tree was visualized using the `ITOL Tree Server` [111].

Structure-based sequence alignment

Chaetomium thermophilum genes encoding ERAD checkpoint proteins were identified through a search of the *Ct* genome with the *Sc*Mnl1/Htm1 (Uniprot P38888) and *Sc*PDI1 (Uniprot P17967) sequences. The searches were carried out using the search tool on the server at https://c-thermophilum.bork.embl.de/. Top hits for the EDEM and PDI were used to search for orthologues using BlastP [112]. The AlphaFold models of the *Ct*EDEM and *Ct*PDI orthologues were downloaded from their Uniprot entry pages.

Structure-based sequence alignment of these sequences was carried out using Salign [53] and the resulting alignment was manually edited. Espript was used to illustrate sequence conservation [113]. The `ConSurf` server at []Yariv:2023ct was used to display sequence conservation on the structure.

Molecular cloning

The DNA sequence encoding Chaetomium thermophilum *Ct*EDEM (Uniprot G0SCX7) was obtained from GeneArt. *Ct*PDI DNA (Uniprot G0SGS2) was amplified

from *Chaetomium thermophilum* cDNA (a gift of Ed Hurt, Biochemistry Centre, Heidelberg University, Heidelberg, Germany). Genes were amplified via PCR using Q5 High-Fidelity Polymerase. Vectors used were Litmus28i for cloning and pHLsec for mammalian expression. Litmus28i was linearized using EcoRI and XhoI, while pHLsec was linearized with AgeI and KpnI.

Primers with 5' overlaps tailored for Gibson assembly were designed. For *Ct*EDEM, a full-length codon-optimized gene was cloned into Litmus28i and pHLsec vectors. The N-terminal GFP fusion construct was generated by amplifying GFP and *Ct*EDEM fragments, followed by Gibson assembly into the pHLsec vector. The DNA sequence encoding for GFP protein was amplified using the plasmid pHLsec:GFP-SLC35B1 (Uniprot ID P78383), kindly donated by Dr Snežana Vasiljević (Biochemistry Department, University of Oxford). For *Ct*PDI, intron removal was achieved by amplifying the two exons separately, excluding the signal peptide and HDEL retrieval signal, and cloning them into pHLsec using Gibson assembly. Gibson assembly reactions were carried out with a 3:1 insert:vector molar ratio and incubated at 50°C for 1 hour. Site-directed mutagenesis of *Ct*PDI was carried out following a protocol outlined in [114]. DNA bands were verified via gel electrophoresis and purified when necessary using the GeneJet Gel Extraction Kit.

Competent DH5α *E. coli* cells were transformed with Gibson assembly products via heat shock and plated on LB agar containing carbenicillin (100 µg/mL). Colony-PCR was performed to confirm successful transformations. Plasmids were purified using GeneJet Miniprep Kits for small-scale preparations and an adapted alkaline lysis protocol for large-scale maxipreps [115]. Purified plasmids were quantified via NanoDrop.

HEK293T transient transfection and Western blot analysis

EDEM3 knock-out HEK293T cells were cultured in DMEM supplemented with 10% FBS and transfected at 65–70% confluence using Polyethylenimine (PEI, 2.5:1 [v/w, PEI:DNA]). Cells were co-transfected with plasmids encoding A1AT-NHK:pCDNA3.1, *Ct*EDEM:pHLsec, *Ct*PDI:pHLsec, *Mm*EDEM3:pcDNA3.1, *Hs*ERp46:pcDNA3.1 controls, using optimized DNA ratios (e.g., 1:1:1 for *Ct*PDI:*Ct*EDEM:NHK triple expression or 3:1 for *Mm*EDEM3:*Hs*ERp46coexpression). For *Hs*ERp46trapping mutant experiments, cells were treated with 10 mM iodoacetamide prior to sampling.

Cells were lysed in Triton X-100 lysis buffer supplemented with protease inhibitors, phosphatase inhibitors, and 20 mM N-ethylmaleimide. Lysates were clarified by centrifugation at 14,000 × g for 20 minutes at 4°C, and protein concentrations were measured using the BCA assay. Equal protein amounts were separated by SDS-PAGE under reducing or non-reducing conditions (6–10% gels depending on the target) and transferred to 0.45 µm nitrocellulose membranes.

Membranes were blocked with 5% milk in TBS and incubated overnight at 4°C with primary antibodies (e.g., anti-A1AT, anti-His, anti-HA, anti-Flag, anti-EDEM3) diluted in 2.5% BSA in TBS. After washing, HRP-conjugated secondary antibodies were applied, and signals were detected using ECL substrate and a ChemiDoc Imaging system (Bio-Rad). Band intensities were quantified with ImageJ (v. 2.1.0) and normalized to the empty vector (EV) control. Statistical analyses were performed using

one-way ANOVA with Dunnett's multiple comparisons test in GraphPad Prism v. 10.1.1. Error bars represent the standard deviation of three independent experiments.

Protein purification

Human embryonic kidney (HEK293F) cells were transfected using the method described in [116]. If multiple plasmids were co-transfected, equal amounts of each plasmid DNA was added.

The HEK293F cell culture was harvested 4 days post-transfection by centrifuging at 4,000 g for 5 minutes. The supernatant containing the secreted protein was adjusted to 1 x PBS pH 7.4 and filtered prior to IMAC. The filtered supernatant was passed onto a 1 mL HisTrap HP Ni IMAC column equilibrated against binding buffer (Na_2HPO_4 50 mM pH 7.5, NaCl 300 mM). The column was washed with 5 column volumes (CV) of wash buffer (Na_2HPO_4 50 mM pH 7.5, NaCl 300 mM, 10 mM imidazole). The proteins were eluted with a 15 CV gradient from 0% to 100% of elution buffer (Na_2HPO_4 50 mM pH 7.5, NaCl 200 mM, 500 mM imidazole.

The protein-containing fractions from IMAC were pooled and concentrated using a polyethersulfone (PES) membrane, 10 kDa MW cutoff centrifugal ultrafiltration device. This sample was then filtered through a 0.2 μm filter and applied to either a Superdex 200 Increase 10/300 GL/Superdex 200 16/600 pg (SEC) or Superdex 200 3.2/300 (microSEC) equilibrated against SEC buffer (HEPES 20 mM pH 7.5, NaCl 100 mM). SDS-PAGE of SEC fractions was used to assess purity (Thermo Fisher NuPAGE Bis-Tris 4-12% gel) and identify fractions of interest for downstream biochemical, structural, and proteomic studies.

Cryo-electron microscopy

Quantifoil Au300 R1.2/1.3 Holey Carbon grids were glow discharged using the EMS GloQube. For non-graphene oxidegrids, settings at 0.2 mBar, 35 mA for 60 seconds were used. For grids to be coated in graphene oxide, settings at 0.2 mBar, 50 mA for 75 seconds). Graphene oxide grid coating was carried out according to the protocol in [117]. Grids were blotted at blot force 10 for 3 seconds before plunge freezing immediately into liquid ethane using a Vitrobot Mark IV.

Cryo-EM data collection

Cryo-EM data collection was carried out on a FEI Titan Krios microscope with Gatan K3 detector at the Midlands Cryo-EM facility using the following settings: acceleration voltage was set to 300 kV; spherical aberration coefficient (Cs) was 2.7 mm; nominal magnification was 105,000x; calibrated pixel size was 0.835 Å; the second condenser aperture was set to 50 µm; the objective aperture was set to 100 µm; the defocus range was from -2.6 µm to -0.7 µm in 0.3 µm intervals; the detector was a K3 (Gatan, USA) in super resolution counting mode binned 2x; the energy filter slide width was 20 eV; the dose rate on the detector was measured over a typical specimen area and was 15 electrons/pixel/s; the dose rate on the specimen was measured over a hole and was 16.5 electrons/pixel/s; the exposure time was 3 sec/micrograph.

Cryo-EM data processing

Data processing was carried out in `RELION 4.0` [118] and cryoSPARC v4.1 [119], with the final *Ct*EDEM:*Ct*PDI reconstruction using cryoSPARC v4.1. In RELION, Motion correction used `MotionCor2` [120], CTF estimation used `CTFFind4` [121] and particle picking was carried out using `Topaz` [122] and autopicking software. In cryoSPARC, patch motion correction and patch CTF estimation were used, and particle used 2D templates from RELION for template picking. 2D classification was carried out in multiple rounds, each time removing particles that gave rise to poor quality classes. *Ab-initio* reconstruction was used to generate multiple initial 3D reconstructions. The various reconstructions were used alongside manufactured junk reconstructions to find and remove further junk particles. 3D classification was used to investigate structural heterogeneity within the dataset, and split particles into subsets. The subsets were refined using homogenous refinement and non-uniform refinement. Reconstructions were improved with local and global CTF refinements. Particle subtraction and local refinements were carried out by first generating masks against the regions of interest using `Create Mask` or `Volume Tools` in `UCSF Chimera` [123]. 3D variability analysis (3DVA) [124] was carried out using a consensus map from non-uniform refinement. 3DVA was run with 3 modes and filter resolution at 6Å. Output mode was set to simple with 20 components. The components of the three modes were visualized and recorded as movies in `Chimera` v1.9 using Volume Series.

Molecular Modelling

Homology models of *Chaetomium thermophilum* protein disulfide isomerase (*Ct*PDI) and ER-degradation enhancing alpha-like mannosidase protein (*Ct*EDEM) in complex were generated using `Alphafold-Multimer` [125]. Sequences were obtained from Uniprot (*Ct*PDI: [G0SGS2], residues 21–505; *Ct*EDEM: [G0SCX7], residues 64–1092) and processed with standard `Alphafold` parameters on the Midlands CryoEM facility computational cluster. Disordered regions with low confidence (local distance difference test score ≤ 75) were removed using a custom pruning script, yielding truncated models for docking into the EM map.

The cryo-EM density maps were generated in `cryoSPARC` and truncated `AlphaFold` maps were docked and refined with `Phenix` [126]. Models were rigid-body fitted with `Phenix.dock_in_map`, and real-space refinements were performed with `Phenix.real_space_refine` [127] using secondary structure and Ramachandran restraints. Missing loops were added iteratively with `Phenix.fit_loops` and manually built in `Coot` [128, 129] where required. Glycosylation sites were modeled using `Coot`'s carbohydrate module, followed by refinement in Phenix.

The `Coot` validation tools `Validate/Ramachandran Plot`, `Validate/Rotamer analysis` and `Validate/Validation Outliers` were used to improve errors in the structure. Favoured side chain rotamers were selected using the `Rotamers` tool. Real-space fit in `Coot` was carried out with Ramachandran restraints and the automated weight calculated by the program for the Cryo-EM map.

Mass spectrometry

SDS-PAGE bands were excised from the gel (approx. 1.5 mm) and washed in ammonium bicarbonate (50 mM, 80 μL, 5 minutes at room temperature) and acetonitrile until all Coomassie stain was removed. Trypsin (15 μL/50 muL) was added to each samples for digestion and incubated at 37 °C overnight.

Tryptic peptides were separated on an Ultimate 3000 RSLC NanoHPLC system Samples were loaded onto a Cartridge based trap column, using a 300 µm x 5 mm C18 PepMap (5 µm, 100 Å) and then separated using Easy-Spray pepMap C18 column (75 µm x 50 cm); with a gradient from 3-10% B in 10 minutes, 10-50% B in 37 minutes, 50-90 % in 9 minutes and 90-3 % in 26 minutes, where mobile phase A was 0.1 % formic acid in water and mobile phase B, 80%/20% ACN/Water in 0.1% formic acid. Flow rate was 0.3 µL/min. The column was operated at a constant temperature of 40 °C. NanoHPLC system was coupled to a Q-Exactive mass spectrometer. The Q-Exactive was operated in the data-dependent top10 mode; full MS scans were acquired at a resolution of 70,000 at m/z 200 to 2000, with an ACG (ion target value) target of 10^6, and a maximum fill time of 50 ms. MS2 scans were acquired at a resolution of 17,500 with an ACG target of 10^5, with a maximum fill time of 100 ms. The dynamic exclusion was set at 30.0 seconds, to prevent repeat sequencing of peptides.

The raw data in mgf format were searched against different combinations of -S-S- linked tryptic peptides obtained from the full sequence of *Ct*EDEM, *Ct*PDI and A1AT-NHK with a tolerance of up to three missed cleavages and using a deviation of up to 0.05 Da for both precursor and peptide fragments. Only MS/MS spectra from precursors of +2 or higher and only full tryptic peptides with a single Cys were considered. Top matches were manually analyzed and confirmed, requiring to contain b and y ions from both of the peptides from the pair.

Plant biology

Plant material and growth conditions

A. thaliana bri1-5 mutant and *mns4-1 mns5-1 bri1-5* triple mutant [44] were grown on soil at 22 °C and 70% relative humidity, under a 16-h-light/8-h-dark cycle (approximately 120 μmol m^{-2} s^{-1}).

Cloning of*Ct*EDEM:eGFP *Ct*EDEM:mRFP

The full-length coding sequence of *Ct*EDEM was amplified by PCR using the Accuprime Pfx DNA Polymerase (Invitrogen), cloned into pDONR™ 221 vector (Invitrogen) and sequenced. DNA primers used for cloning are "*Ct*EDEM_pDONR™ 221" in Table S1. Full-length *Ct*EDEM was then cloned using the Gateway® Technology into two destination vectors, pB7RWG2 and pK7WGF2

Binary vectors, containing the constructs, were amplified in *Escherichia coli* DH5α before transformation of *Agrobacterium tumefaciens* (strain GV3101).

Plant stable transformation

Later, the constructs *Ct*EDEM:mRFP and *Ct*EDEM:eGFP were used for stable transformation of the *A. thaliana mns4-1/mns5-1/bri1-5* triple mutant. *Arabidopsis* plants were transformed using the floral dip method [130]. Healthy *Arabidopsis* plants were grown until they were flowering. *Agrobacterium tumefaciens* carrying gene *Ct*EDEM was spun down and resuspended to OD_{600}=0.8 in 500 mL of 5% Sucrose, 10 mM $MgCl_2$, 200 μM acetosyringone. Before dipping, Silwet L-77 was added to a concentration of 0.05% (500 μL/L). *At* was dipped in *Agrobacterium* solution for 1 minute and kept under cover for 48 hours to maintain high humidity. After 5 days, the dipping procedure was repeated. Dry seeds were harvested and the transformants were selected on 1/2 MS medium with phosphinothricin (aka Basta, Duchefa P0159) for *Ct*EDEM:mRFP plants, with kanamycin for *Ct*EDEM:eGFP plants.

Confocal Laser Scanning Microscopy and *Ct*EDEM expression and localisation *in planta*

Confocal images were taken by a laser-scanning confocal microscope (LSM Pascal; Carl Zeiss). *Ct*EDEM:eGFP signal was excited at 488 nm with an argon laser and detected with a 505–530 nm filter set; whereas *Ct*EDEM:mRFP was excited at 543 nm with a He/Ne laser and detected in the 560–615 nm range. Chlorophyll autofluorescence was detected with the filter $>$ 650 nm.

Declarations

Acknowledgements

We thank Radu Aricescu and Ed Hurt for donating the pHLsec vector and the *Ct* cDNA library, respectively. We acknowledge T.J. Ragan and the Midlands Regional CryoEM Facility at the Leicester Institute of Structural and Chemical Biology (LISCB), major funding from MRC (MC_PC_17136).

Funding

C.J.H. was the recipient of an MRC IMPACT Programme Studentship and supported by the Membrane Protein Laboratory (funded by grant 223727/Z/21/Z from the Wellcome Trust) at the Diamond Light Source Ltd and Research Complex at Harwell. A.L. was the recipient of a PhD Studentship from the Agricultural and Forestry Department (DAFNE) of the University of Tuscia (Viterbo, Italy) and funding from the Italian National Research Council (to A.S.). P.R. was the recipient of an LISCB Wellcome Trust ISSF award, grant reference 204801/Z/16/Z and a Wellcome Trust Seed Award in Science, grant reference 214090/Z/18/Z. A.S. and P.R. were the recipients of a Research Project Prize 2021 (Grant code `Plant_EDEM` by the Department of Biological and Agro-alimentary Sciences of the Italian National Research Council). P.R. and S.P. were joint recipients of a bilateral grant from the Italian National Research Council and the Romanian Academy of Sciences. B.G. is funded by the Alpha-1 Foundation and the NIHR Leicester Biomedical Research Centre (BRC).

Conflict of interest/Competing interests:

The authors declare no competing interests.

Data availability

Structure coordinates were deposited to the Research Collaboratory for Structural Bioinformatics PDB (https://www.rcsb.org/) and cryo-EM density maps used in model building were deposited to the EM Data Bank (https://www.ebi.ac.uk/pdbe/emdb) under the following accession codes: 8PKO and EMD-17749. Other data supporting the findings of this study are available from the corresponding authors on request.

Author contributions

C.J.H. and A.L. contributed equally to this work. P.R., A.S., B.G. and N.H. conceived and resourced the study. P.R. and A.L. cloned the *Ct*EDEM and *Ct*PDI DNA constructs. P.R., G.T. and C.J.H. purified protein. C.J.H. prepared Cryo-EM grids. C.S. and C.J.H. collected Cryo-EM data. C.J.H processed Cryo-EM data. P.R., Y.B., I.C. and C.J.H. built and refined the structural model. A.S., M.D.B. and A.L. carried out the experiments with *Ct*EDEM in plants. C.J.H, B.G, and A.Q planned and carried out the A1AT-NHK ternary complex cryo-EM studies and conducted the *Ct*PDI trapping mutant studies. N.H., I.W., S.G., S.P., G.N.C. and C.V.A.M. carried out the in

gel Western Blot experiments. P.R., N.H., I.W., C.J.H. and C.V.A.M. planned the MS experiments. C.J.H. and C.V.A.M. analysed the MS data. J.R.O. and C.P.M. carried out the phylogenetic analysis. I.W. and N.H. carried out the experiments with *Hs*EDEM3 and *Mm*ERp46. All authors contributed to the writing of the manuscript.

References

[1] Helenius, A., Aebi, M.: Roles of n-linked glycans in the endoplasmic reticulum. Annual Review of Biochemistry **73**(1), 1019–1049 (2004) https://doi.org/10.1146/annurev.biochem.73.011303.073752 https://doi.org/10.1146/annurev.biochem.73.011303.073752. PMID: 15189166

[2] Berner, N., Reutter, K.-R., Wolf, D.H.: Protein quality control of the endoplasmic reticulum and ubiquitin–proteasome-triggered degradation of aberrant proteins: Yeast pioneers the path. Annual Review of Biochemistry **87**(Volume 87, 2018), 751–782 (2018) https://doi.org/10.1146/annurev-biochem-062917-012749

[3] Sun, Z., Brodsky, J.L.: Protein quality control in the secretory pathway. The Journal of cell biology **218**(10), 3171–3187 (2019)

[4] Christianson, J.C., Jarosch, E., Sommer, T.: Mechanisms of substrate processing during ER-associated protein degradation. Nature Reviews Molecular Cell Biology **24**(11), 777–796 (2023) https://doi.org/10.1038/s41580-023-00633-8

[5] Gooptu, B., Dickens, J.A., Lomas, D.A.: The molecular and cellular pathology of α1-antitrypsin deficiency. Trends in Molecular Medicine **20**(2), 116–127 (2014) https://doi.org/10.1016/j.molmed.2013.10.007

[6] Wang, M., Kaufman, R.J.: Protein misfolding in the endoplasmic reticulum as a conduit to human disease. Nature **529**(7586), 326–335 (2016) https://doi.org/10.1038/nature17041

[7] Wiseman, R.L., Mesgarzadeh, J.S., Hendershot, L.M.: Reshaping endoplasmic reticulum quality control through the unfolded protein response. Molecular Cell **82**(8), 1477–1491 (2022) https://doi.org/10.1016/j.molcel.2022.03.025

[8] Marciniak, S.J., Chambers, J.E., Ron, D.: Pharmacological targeting of endoplasmic reticulum stress in disease. Nature Reviews Drug Discovery **21**(2), 115–140 (2022) https://doi.org/10.1038/s41573-021-00320-3

[9] Acosta-Alvear, D., Harnoss, J.M., Walter, P., Ashkenazi, A.: Homeostasis control in health and disease by the unfolded protein response. Nat Rev Mol Cell Biol (2024) https://doi.org/10.1038/s41580-024-00794-0

[10] Bigi, A., Lombardo, E., Cascella, R., Cecchi, C.: The toxicity of protein aggregates: New insights into the mechanisms. International Journal of Molecular Sciences **24**(9) (2023) https://doi.org/10.3390/ijms24097974

[11] Chen, G., Wei, T., Ju, F., Li, H.: Protein quality control and aggregation in the endoplasmic reticulum: From basic to bedside. Frontiers in Cell and Developmental Biology **11** (2023) https://doi.org/10.3389/fcell.2023.1156152

[12] Marciniak, S.J., Ron, D.: Endoplasmic reticulum stress signaling in disease. Physiological Reviews (2006) https://doi.org/10.1152/physrev.00015.2006.-The

[13] Bhattacharya, A., Qi, L.: ER-associated degradation in health and disease – from substrate to organism. Journal of Cell Science **132**(23) (2019)

[14] S, G., M, C., R, T., A, M.-V., SM, P.: Targeting edem protects against er stress and improves development and survival in c. elegans. PLoS Genetics **18** (2022) https://doi.org/10.1371/journal.pgen.1010069

[15] Clerc, S., Hirsch, C., Oggier, D.M., Deprez, P., Jakob, C., Sommer, T., Aebi, M.: Htm1 protein generates the N-glycan signal for glycoprotein degradation in the endoplasmic reticulum. The Journal of cell biology **184**(1), 159–172 (2009)

[16] Hosokawa, N., Tremblay, L.O., Sleno, B., Kamiya, Y., Wada, I., Nagata, K., Kato, K., Herscovics, A.: EDEM1 accelerates the trimming of α1,2-linked mannose on the C branch of N-glycans. Glycobiology **20**(5), 567–575 (2010) https://doi.org/10.1093/glycob/cwq001 https://academic.oup.com/glycob/article-pdf/20/5/567/5845559/cwq001.pdf

[17] George, G., Ninagawa, S., Yagi, H., Saito, T., Ishikawa, T., Sakuma, T., Yamamoto, T., Imami, K., Ishihama, Y., Kato, K., Okada, T., Mori, K.: EDEM2 stably disulfide-bonded to TXNDC11 catalyzes the first mannose trimming step in mammalian glycoprotein ERAD. eLife **9** (2020)

[18] Zhang, J., Wu, J., Liu, L., Li, J.: The crucial role of demannosylating asparagine-linked glycans in eradicating misfolded glycoproteins in the endoplasmic reticulum. Frontiers in Plant Science **11** (2021) https://doi.org/10.3389/fpls.2020.625033 . Cited by: 6; All Open Access, Gold Open Access, Green Open Access

[19] Su, K., Stoller, T., Rocco, J., Zemsky, J., Green, R.: Pre-Golgi degradation of yeast prepro-alpha-factor expressed in a mammalian cell. Influence of cell type-specific oligosaccharide processing on intracellular fate. The Journal of biological chemistry **268**(19), 14301–14309 (1993)

[20] Pisoni, G.B., Molinari, M.: Five Questions (with their Answers) on ER-Associated Degradation. Traffic (Copenhagen, Denmark) **17**(4), 341–350 (2016)

[21] Vembar, S.S., Brodsky, J.L.: One step at a time: endoplasmic reticulum-associated degradation. Nature reviews. Molecular cell biology **9**(12), 944–957 (2008)

[22] Brodsky, J.: Cleaning up: Er-associated degradation to the rescue. Cell **151**(6), 1163–1167 (2012) https://doi.org/10.1016/j.cell.2012.11.012

[23] Wu, X., Rapoport, T.A.: Mechanistic insights into er-associated protein degradation. Current Opinion in Cell Biology **53**, 22–28 (2018) https://doi.org/10.1016/j.ceb.2018.04.004 . Membrane Trafficking

[24] Krshnan, L., Weijer, M.L., Carvalho, P.: Endoplasmic reticulum-associated protein degradation. Cold Spring Harb Perspect Biol **14**(12) (2022) https://doi.org/10.1101/cshperspect.a041247

[25] Sakoh-Nakatogawa, M., Nishikawa, S.-I., Endo, T.: Roles of protein-disulfide isomerase-mediated disulfide bond formation of yeast Mnl1p in endoplasmic reticulum-associated degradation. The Journal of biological chemistry **284**(18), 11815–11825 (2009)

[26] Liu, Y.-C., Fujimori, D.G., Weissman, J.S.: Htm1p–pdi1p is a folding-sensitive mannosidase that marks n-glycoproteins for er-associated protein degradation. Proceedings of the National Academy of Sciences **113**(28), 4015–4024 (2016) https://doi.org/10.1073/pnas.1608795113 https://www.pnas.org/content/113/28/E4015.full.pdf

[27] Gauss, R., Kanehara, K., Carvalho, P., Ng, D.T.W., Aebi, M.: A complex of Pdi1p and the mannosidase Htm1p initiates clearance of unfolded glycoproteins from the endoplasmic reticulum. Molecular Cell **42**(6), 782–793 (2011)

[28] Zhao, D., Wu, X., Rapoport, T.A.: Initiation of erad by the bifunctional complex of mnl1 mannosidase and protein disulfide isomerase. bioRxiv (2024) https://doi.org/10.1101/2024.10.17.618908 https://www.biorxiv.org/content/early/2024/10/17/2024.10.17.618908.full.pdf

[29] Hosokawa, N., Wada, I., Hasegawa, K., Yorihuzi, T., Tremblay, L.O., Herscovics, A., Nagata, K.: A novel ER alpha-mannosidase-like protein accelerates ER-associated degradation. EMBO reports **2**(5), 415–422 (2001)

[30] Mast, S.W., Diekman, K., Karaveg, K., Davis, A., Sifers, R.N., Moremen, K.W.: Human EDEM2, a novel homolog of family 47 glycosidases, is involved in ER-associated degradation of glycoproteins. Glycobiology **15**(4), 421–436 (2004) https://doi.org/10.1093/glycob/cwi014 . _eprint: https://academic.oup.com/glycob/article-pdf/15/4/421/17485728/cwi014.pdf

[31] Olivari, S., Galli, C., Alanen, H., Ruddock, L., Molinari, M.: A novel stress-induced EDEM variant regulating endoplasmic reticulum-associated glycoprotein degradation. The Journal of biological chemistry **280**(4), 2424–2428 (2005)

[32] Hirao, K., Natsuka, Y., Tamura, T., Wada, I., Morito, D., Natsuka, S., Romero, P., Sleno, B., Tremblay, L.O., Herscovics, A., Nagata, K., Hosokawa, N.: EDEM3, a soluble EDEM homolog, enhances glycoprotein endoplasmic

reticulum-associated degradation and mannose trimming. The Journal of biological chemistry **281**(14), 9650–9658 (2006)

[33] Ushioda, R., Hoseki, J., Araki, K., Jansen, G., Thomas, D.Y., Nagata, K.: Erdj5 is required as a disulfide reductase for degradation of misfolded proteins in the er. Science **321**(5888), 569–572 (2008) https://doi.org/10.1126/science.1159293 https://science.sciencemag.org/content/321/5888/569.full.pdf

[34] Hagiwara, M., Maegawa, K.-I., Suzuki, M., Ushioda, R., Araki, K., Matsumoto, Y., Hoseki, J., Nagata, K., Inaba, K.: Structural basis of an ERAD pathway mediated by the ER-resident protein disulfide reductase ERdj5. Molecular cell **41**(4), 432–444 (2011)

[35] Timms, R.T., Menzies, S.A., Tchasovnikarova, I.A., Christensen, L.C., Williamson, J.C., Antrobus, R., Dougan, G., Ellgaard, L., Lehner, P.J.: Genetic dissection of mammalian erad through comparative haploid and crispr forward genetic screens. Nature Communications **7**(1), 11786 (2016) https://doi.org/10.1038/ncomms11786

[36] Shenkman, M., Ron, E., Yehuda, R., Benyair, R., Khalaila, I., Lederkremer, G.Z.: Mannosidase activity of EDEM1 and EDEM2 depends on an unfolded state of their glycoprotein substrates. Communications biology **1**(1), 172 (2018)

[37] Yu, S., Ito, S., Wada, I., Hosokawa, N.: Er-resident protein 46 (erp46) triggers the mannose-trimming activity of er degradation–enhancing α-mannosidase–like protein 3 (edem3). Journal of Biological Chemistry **293**(27), 10663–10674 (2018) https://doi.org/10.1074/jbc.RA118.003129

[38] Hebert, D.N., Molinari, M.: In and out of the ER: Protein folding, quality control, degradation, and related human diseases. Physiological Reviews **87**(4), 1377–1408 (2007) https://doi.org/10.1152/physrev.00050.2006

[39] Hebert, D.N., Lamriben, L., Powers, E.T., Kelly, J.W.: The intrinsic and extrinsic effects of N-linked glycans on glycoproteostasis. Nature Chemical Biology **10**(11), 902–910 (2014)

[40] Duwaerts, C.C., Maiers, J.L.: ER Disposal Pathways in Chronic Liver Disease: Protective, Pathogenic, and Potential Therapeutic Targets. Frontiers in molecular biosciences **8**, 804097 (2021)

[41] Quirke, J.C.K., Crich, D.: GH47 and Other Glycoside Hydrolases Catalyze Glycosidic Bond Cleavage with the Assistance of Substrate Super-arming at the Transition State. ACS catalysis **11**, 10308–10315 (2021)

[42] Sobala, Ł.F., Fernandes, P.Z., Hakki, Z., Thompson, A.J., Howe, J.D., Hill, M., Zitzmann, N., Davies, S., Stamataki, Z., Butters, T.D., Alonzi, D.S., Williams, S.J., Davies, G.J.: Structure of human endo-α-1,2-mannosidase (MANEA), an

antiviral host-glycosylation target. Proceedings of the National Academy of Sciences of the United States of America **117**(47), 29595–29601 (2020)

[43] Lynch, M.: Gene duplication and evolution. In: Evolution From Molecules to Ecosystems. Oxford University Press, ??? (2004). https://doi.org/10.1093/oso/9780198515425.003.0004 . https://doi.org/10.1093/oso/9780198515425.003.0004

[44] Hüttner, S., Veit, C., Vavra, U., Schoberer, J., Liebminger, E., Maresch, D., Grass, J., Altmann, F., Mach, L., Strasser, R.: Arabidopsis class i α-mannosidases MNS4 and MNS5 are involved in endoplasmic reticulum–associated degradation of misfolded glycoproteins. The Plant Cell **26**(4), 1712–1728 (2014) https://doi.org/10.1105/tpc.114.123216

[45] Ruddock, L.W., Molinari, M.: N-glycan processing in er quality control. J Cell Sci **119**(Pt 21), 4373–4380 (2006) https://doi.org/10.1242/jcs.03225

[46] Balaji, S., Srinivasan, N.: Comparison of sequence-based and structure-based phylogenetic trees of homologous proteins: Inferences on protein evolution. Journal of Biosciences **32**(1), 83–96 (2007) https://doi.org/10.1007/s12038-007-0008-1

[47] Malik, A.J., Poole, A.M., Allison, J.R.: Structural phylogenetics with confidence. Molecular Biology and Evolution **37**(9), 2711–2726 (2020) https://doi.org/10.1093/molbev/msaa100 https://academic.oup.com/mbe/article-pdf/37/9/2711/33866729/msaa100.pdf

[48] Kempen, M., Kim, S.S., Tumescheit, C., Mirdita, M., Lee, J., Gilchrist, C.L.M., Söding, J., Steinegger, M.: Fast and accurate protein structure search with foldseek. Nature Biotechnology **42**(2), 243–246 (2024) https://doi.org/10.1038/s41587-023-01773-0

[49] Manica, G., Ghenea, S., Munteanu, C.V.A., Martin, E.C., Butnaru, C., Surleac, M., Chiritoiu, G.N., Alexandru, P.R., Petrescu, A.-J., Petrescu, S.M.: Edem3 domains cooperate to perform its overall cell functioning. International Journal of Molecular Sciences **22**(4) (2021) https://doi.org/10.3390/ijms22042172

[50] Krogh, A., Larsson, B., von Heijne, G., Sonnhammer, E.L.L.: Predicting transmembrane protein topology with a hidden markov model: application to complete genomes11edited by f. cohen. Journal of Molecular Biology **305**(3), 567–580 (2001) https://doi.org/10.1006/jmbi.2000.4315

[51] Ushioda, R., Hoseki, J., Nagata, K.: Glycosylation-independent erad pathway serves as a backup system under er stress. Mol Biol Cell **24**(20), 3155–3163 (2013) https://doi.org/10.1091/mbc.E13-03-0138

[52] Lamriben, L., Oster, M.E., Tamura, T., Tian, W., Yang, Z., Clausen, H., Hebert,

D.N.: Edem1's mannosidase-like domain binds erad client proteins in a redox-sensitive manner and possesses catalytic activity. J Biol Chem **293**(36), 13932–13945 (2018) https://doi.org/10.1074/jbc.RA118.004183

[53] Ayub, U., Haider, I., Naveed, H.: SAlign–a structure aware method for global PPI network alignment. BMC Bioinformatics **21**(1), 500 (2020)

[54] Jumper, J., Evans, R., Pritzel, A., Green, T., Figurnov, M., Ronneberger, O., Tunyasuvunakool, K., Bates, R., Žídek, A., Potapenko, A., Bridgland, A., Meyer, C., Kohl, S.A.A., Ballard, A.J., Cowie, A., Romera-Paredes, B., Nikolov, S., Jain, R., Adler, J., Back, T., Petersen, S., Reiman, D., Clancy, E., Zielinski, M., Steinegger, M., Pacholska, M., Berghammer, T., Silver, D., Vinyals, O., Senior, A.W., Kavukcuoglu, K., Kohli, P., Hassabis, D.: Applying and improving AlphaFold at CASP14. Proteins **89**(12), 1711–1721 (2021)

[55] Leuenberger, P., Ganscha, S., Kahraman, A., Cappelletti, V., Boersema, P.J., Mering, C., Claassen, M., Picotti, P.: Cell-wide analysis of protein thermal unfolding reveals determinants of thermostability. Science **355**(6327), 7825 (2017) https://doi.org/10.1126/science.aai7825 https://www.science.org/doi/pdf/10.1126/science.aai7825

[56] Hüttner, S., Veit, C., Schoberer, J., Grass, J., Strasser, R.: Unraveling the function of arabidopsis thaliana OS9 in the endoplasmic reticulum-associated degradation of glycoproteins. Plant Molecular Biology **79**(1-2), 21–33 (2012) https://doi.org/10.1007/s11103-012-9891-4

[57] Ronzoni, R., Berardelli, R., Medicina, D., Sitia, R., Gooptu, B., Fra, A.M.: Aberrant disulphide bonding contributes to the er retention of alpha1-antitrypsin deficiency variants. Human Molecular Genetics **25**(4), 642–650 (2015) https://doi.org/10.1093/hmg/ddv501 https://academic.oup.com/hmg/article-pdf/25/4/642/18526797/ddv501.pdf

[58] Vagin, A., Teplyakov, A.: Molecular replacement with MOLREP. Acta crystallographica. Section D, Biological crystallography **66**(Pt 1), 22–25 (2010)

[59] Chen, V.B., Arendall, W.B.r., Headd, J.J., Keedy, D.A., Immormino, R.M., Kapral, G.J., Murray, L.W., Richardson, J.S., Richardson, D.C.: Molprobity: all-atom structure validation for macromolecular crystallography. Acta Crystallogr D Biol Crystallogr **66**(Pt 1), 12–21 (2010) https://doi.org/10.1107/S0907444909042073

[60] Alexander, L.T., Durairaj, J., Kryshtafovych, A., Abriata, L.A., Bayo, Y., Bhabha, G., Breyton, C., Caulton, S.G., Chen, J., Degroux, S., Ekiert, D.C., Erlandsen, B.S., Freddolino, P.L., Gilzer, D., Greening, C., Grimes, J.M., Grinter, R., Gurusaran, M., Hartmann, M.D., Hitchman, C.J., Keown, J.R., Kropp, A., Kursula, P., Lovering, A.L., Lemaitre, B., Lia, A., Liu, S., Logotheti, M., Lu, S., Markússon, S., Miller, M.D., Minasov, G., Niemann, H.H., Opazo, F.,

Phillips, G.N.J., Davies, O.R., Rommelaere, S., Rosas-Lemus, M., Roversi, P., Satchell, K., Smith, N., Wilson, M.A., Wu, K.-L., Xia, X., Xiao, H., Zhang, W., Zhou, Z.H., Fidelis, K., Topf, M., Moult, J., Schwede, T.: Protein target highlights in casp15: Analysis of models by structure providers. Proteins **91**(12), 1571–1599 (2023) https://doi.org/10.1002/prot.26545

[61] Vallée, F., Karaveg, K., Herscovics, A., Moremen, K.W., Howell, P.L.: Structural basis for catalysis and inhibition of N-glycan processing class I alpha 1,2-mannosidases. Journal of Biological Chemistry **275**(52), 41287–41298 (2000)

[62] Vallée, F., Lipari, F., Yip, P., Sleno, B., Herscovics, A., Howell, P.L.: Crystal structure of a class I alpha1,2-mannosidase involved in N-glycan processing and endoplasmic reticulum quality control. The EMBO Journal **19**(4), 581–588 (2000)

[63] Olivari, S., Cali, T., Salo, K.E.H., Paganetti, P., Ruddock, L.W., Molinari, M.: EDEM1 regulates ER-associated degradation by accelerating de-mannosylation of folding-defective polypeptides and by inhibiting their covalent aggregation. Biochemical and Biophysical Research Communications **349**(4), 1278–1284 (2006) https://doi.org/10.1016/j.bbrc.2006.08.186

[64] Ninagawa, S., Okada, T., Sumitomo, Y., Kamiya, Y., Kato, K., Horimoto, S., Ishikawa, T., Takeda, S., Sakuma, T., Yamamoto, T., Mori, K.: EDEM2 initiates mammalian glycoprotein ERAD by catalyzing the first mannose trimming step. The Journal of cell biology **206**(3), 347–356 (2014)

[65] Xiang, Y., Karaveg, K., Moremen, K.W.: Substrate recognition and catalysis by GH47 α-mannosidases involved in Asn-linked glycan maturation in the mammalian secretory pathway. Proceedings of the National Academy of Sciences of the United States of America **113**(49), 7890–7899 (2016)

[66] Holm, L., Rosenström, P.: Dali server: conservation mapping in 3D. Nucleic acids research **38**(Web Server issue), 545–9 (2010)

[67] Pfeiffer, A., Stephanowitz, H., Krause, E., Volkwein, C., Hirsch, C., Jarosch, E., Sommer, T.: A Complex of Htm1 and the Oxidoreductase Pdi1 Accelerates Degradation of Misfolded Glycoproteins. The Journal of biological chemistry **291**(23), 12195–12207 (2016)

[68] Molinari, M.: Role of EDEM in the release of misfolded glycoproteins from the calnexin cycle. Science **299**(5611), 1397–1400 (2003) https://doi.org/10.1126/science.1079474

[69] Oda, Y., Hosokawa, N., Wada, I., Nagata, K.: EDEM as an acceptor of terminally misfolded glycoproteins released from calnexin. Science (New York, N.Y.) **299**(5611), 1394–1397 (2003)

[70] Mast, S.W., Diekman, K., Karaveg, K., Davis, A., Sifers, R.N., Moremen, K.W.: Human EDEM2, a novel homolog of family 47 glycosidases, is involved in ER-associated degradation of glycoproteins. Glycobiology **15**(4), 421–436 (2005)

[71] Tempel, W., Karaveg, K., Liu, Z.-J., Rose, J., Wang, B.-C., Moremen, K.W.: Structure of mouse golgi α-mannosidase ia reveals the molecular basis for substrate specificity among class 1 (family 47 glycosylhydrolase) α1,2-mannosidases*. Journal of Biological Chemistry **279**(28), 29774–29786 (2004) https://doi.org/10.1074/jbc.M403065200

[72] Bedem, H., Wilson, M.A.: Shining light on cysteine modification: connecting protein conformational dynamics to catalysis and regulation. Journal of Synchrotron Radiation **26**(4), 958–966 (2019) https://doi.org/10.1107/S160057751900568X

[73] Tempel, W., Karaveg, K., Liu, Z.-J., Rose, J., Wang, B.-C., Moremen, K.W.: Structure of mouse golgiα-mannosidase ia reveals the molecular basis for substrate specificity among class 1 (family 47 glycosylhydrolase) 1,2-mannosidases*. Journal of Biological Chemistry **279**(28), 29774–29786 (2004) https://doi.org/10.1074/jbc.M403065200

[74] Chinnaraj, M., Flaumenhaft, R., Pozzi, N.: Reduction of protein disulfide isomerase results in open conformations and stimulates dynamic exchange between structural ensembles. Journal of Biological Chemistry **298**(8), 102217 (2022) https://doi.org/10.1016/J.JBC.2022.102217

[75] Yagi-Utsumi, M., Miura, H., Ganser, C., Watanabe, H., Hiranyakorn, M., Satoh, T., Uchihashi, T., Kato, K., Okazaki, K.-i., Aoki, K.: Molecular design of fret probes based on domain rearrangement of protein disulfide isomerase for monitoring intracellular redox status. International Journal of Molecular Sciences **24**(16) (2023) https://doi.org/10.3390/ijms241612865

[76] Lyles, M.M., Gilbert, H.F.: Mutations in the thioredoxin sites of protein disulfide isomerase reveal functional nonequivalence of the n- and c-terminal domains. J Biol Chem **269**(49), 30946–30952 (1994)

[77] Pandhare, J., Deshpande, V.: Both chaperone and isomerase functions of protein disulfide isomerase are essential for acceleration of the oxidative refolding and reactivation of dimeric alkaline protease inhibitor. Protein Sci **13**(9), 2493–2501 (2004) https://doi.org/10.1110/ps.03552004

[78] Sokołowska, I., Piłka, E.S., Sandvig, K., Wegrzyn, G., Slomińska-Wojewódzka, M.: Hydrophobicity of protein determinants influences the recognition of substrates by EDEM1 and EDEM2 in human cells. BMC Cell Biology **16**(1), 1–18 (2015) https://doi.org/10.1186/s12860-015-0047-7

[79] Georgescauld, F., Popova, K., Gupta, A.J., Bracher, A., Engen, J.R., Hayer-Hartl, M., Hartl, F.U.: Groel/es chaperonin modulates the mechanism and

accelerates the rate of tim-barrel domain folding. Cell **157**, 922–934 (2014) https://doi.org/10.1016/j.cell.2014.03.038

[80] Pobre, K.F.R., Poet, G.J., Hendershot, L.M.: The endoplasmic reticulum (er) chaperone bip is a master regulator of er functions: Getting by with a little help from erdj friends. Journal of Biological Chemistry **294**, 2098–2108 (2019) https://doi.org/10.1074/jbc.REV118.002804

[81] Ninagawa, S., Matsuo, M., Ying, D., Oshita, S., Aso, S., Matsushita, K., Taniguchi, M., Fueki, A., Yamashiro, M., Sugasawa, K., Saito, S., Imami, K., Kizuka, Y., Sakuma, T., Yamamoto, T., Yagi, H., Kato, K., Mori, K.: Uggt1-mediated reglucosylation of n-glycan competes with er-associated degradation of unstable and misfolded glycoproteins. Elife **12** (2024) https://doi.org/10.7554/eLife.93117

[82] Wang, N., Seko, A., Takeda, Y., Ito, Y.: Glycan dependent refolding activity of er glucosyltransferase (uggt). Biochim Biophys Acta Gen Subj **1864**(12), 129709 (2020) https://doi.org/10.1016/j.bbagen.2020.129709

[83] Modenutti, C.P., Capurro, J.I.B., Ibba, R., Alonzi, D.S., Song, M.N., Vasiljević, S., Kumar, A., Chandran, A.V., Tax, G., Marti, L., Hill, J.C., Lia, A., Hensen, M., Waksman, T., Rushton, J., Rubichi, S., Santino, A., Martí, M.A., Zitzmann, N., Roversi, P.: Clamping, bending, and twisting inter-domain motions in the misfold-recognizing portion of udp-glucose: Glycoprotein glucosyltransferase. Structure **29**, 357–3709 (2021) https://doi.org/10.1016/j.str.2020.11.017

[84] Williams, R.V., Guay, K.P., Hurlbut Lesk, O.A., Clerico, E.M., Hebert, D.N., Gierasch, L.M.: Insights into the interaction between uggt, the gatekeeper of folding in the er, and its partner, the selenoprotein sep15. Proc Natl Acad Sci U S A **121**(34), 2315009121 (2024) https://doi.org/10.1073/pnas.2315009121

[85] Taylor, S.C., Thibault, P., Tessier, D.C., Bergeron, J.J.M., Thomas, D.Y.: Glycopeptide specificity of the secretory protein folding sensor udp-glucose glycoprotein:glucosyltransferase. EMBO Rep **4**(4), 405–411 (2003) https://doi.org/10.1038/sj.embor.embor797

[86] Izumi, M., Kuruma, R., Okamoto, R., Seko, A., Ito, Y., Kajihara, Y.: Substrate recognition of glycoprotein folding sensor uggt analyzed by site-specifically 15n-labeled glycopeptide and small glycopeptide library prepared by parallel native chemical ligation. Journal of the American Chemical Society **139**(33), 11421–11426 (2017) https://doi.org/10.1021/jacs.7b03277

[87] Hebditch, M., Warwicker, J.: Web-based display of protein surface and pH-dependent properties for assessing the developability of biotherapeutics. Scientific Reports **9**(1), 1–9 (2019) https://doi.org/10.1038/s41598-018-36950-8

[88] Meng, E.C., Goddard, T.D., Pettersen, E.F., Couch, G.S., Pearson, Z.J.,

Morris, J.H., Ferrin, T.E.: Ucsf chimerax: Tools for structure building and analysis. Protein Science **32**(11), 4792 (2023) https://doi.org/10.1002/pro.4792 https://onlinelibrary.wiley.com/doi/pdf/10.1002/pro.4792

[89] Kozlov, G., Määttänen, P., Thomas, D.Y., Gehring, K.: A structural overview of the PDI family of proteins. FEBS Journal **277**(19), 3924–3936 (2010) https://doi.org/10.1111/j.1742-4658.2010.07793.x

[90] Molinari, M., Galli, C., Piccaluga, V., Pieren, M., Paganetti, P.: Sequential assistance of molecular chaperones and transient formation of covalent complexes during protein degradation from the ER. The Journal of cell biology **158**(2), 247–257 (2002)

[91] Hatahet, F., Ruddock, L.W.: Substrate recognition by the protein disulfide isomerases. The FEBS Journal **274**(20), 5223–5234 (2007) https://doi.org/10.1111/j.1742-4658.2007.06058.x https://febs.onlinelibrary.wiley.com/doi/pdf/10.1111/j.1742-4658.2007.06058.x

[92] Jessop, C.E., Chakravarthi, S., Garbi, N., Hämmerling, G.J., Lovell, S., Bulleid, N.J.: Erp57 is essential for efficient folding of glycoproteins sharing common structural domains. The EMBO Journal **26**(1), 28–40 (2007) https://doi.org/10.1038/sj.emboj.7601505 https://www.embopress.org/doi/pdf/10.1038/sj.emboj.7601505

[93] Jessop, C.E., Watkins, R.H., Simmons, J.J., Tasab, M., Bulleid, N.J.: Protein disulphide isomerase family members show distinct substrate specificity: P5 is targeted to BiP client proteins. Journal of cell science **122**(Pt 23), 4287–4295 (2009)

[94] Juszkiewicz, S., Hegde, R.S.: Quality control of orphaned proteins. Molecular Cell **71**, 443–457 (2018) https://doi.org/10.1016/j.molcel.2018.07.001 . doi: 10.1016/j.molcel.2018.07.001

[95] George, G., Ninagawa, S., Yagi, H., Furukawa, J.-i., Hashii, N., Ishii-Watabe, A., Deng, Y., Matsushita, K., Ishikawa, T., Mamahit, Y.P., Maki, Y., Kajihara, Y., Kato, K., Okada, T., Mori, K.: Purified edem3 or edem1 alone produces determinant oligosaccharide structures from m8b in mammalian glycoprotein erad. eLife **10**, 70357 (2021) https://doi.org/10.7554/eLife.70357

[96] Chiu, J., Hogg, P.J.: Allosteric disulfides: Sophisticated molecular structures enabling flexible protein regulation. J Biol Chem **294**(8), 2949–2960 (2019) https://doi.org/10.1074/jbc.REV118.005604

[97] Lipari, F., Herscovics, A.: Role of the cysteine residues in the alpha1,2-mannosidase involved in n-glycan biosynthesis in saccharomyces cerevisiae. the conserved cys340 and cys385 residues form an essential disulfide bond. J Biol Chem **271**(44), 27615–27622 (1996) https://doi.org/10.1074/jbc.271.44.27615

[98] Maegawa, K.-i., Watanabe, S., Noi, K., Okumura, M., Amagai, Y., Inoue, M., Ushioda, R., Nagata, K., Ogura, T., Inaba, K.: The highly dynamic nature of erdj5 is key to efficient elimination of aberrant protein oligomers through er-associated degradation. Structure **25**(6), 846–8574 (2017) https://doi.org/10.1016/j.str.2017.04.001

[99] Ushioda, R., Nagata, K.: Redox-mediated regulatory mechanisms of endoplasmic reticulum homeostasis. Cold Spring Harb Perspect Biol **11**(5) (2019) https://doi.org/10.1101/cshperspect.a033910

[100] Patel, C., Saad, H., Shenkman, M., Lederkremer, G.Z.: Oxidoreductases in glycoprotein glycosylation, folding, and ERAD. Cells **9**(9), 2138 (2020) https://doi.org/10.3390/cells9092138

[101] Kojima, R., Okumura, M., Masui, S., Kanemura, S., Inoue, M., Saiki, M., Yamaguchi, H., Hikima, T., Suzuki, M., Akiyama, S., Inaba, K.: Radically Different Thioredoxin Domain Arrangement of ERp46, an Efficient Disulfide Bond Introducer of the Mammalian PDI Family. Structure/Folding and Design **22**(3), 431–443 (2014)

[102] Su, C.-C., Lyu, M., Zhang, Z., Miyagi, M., Huang, W., Taylor, D.J., Yu, E.W.: High-resolution structural-omics of human liver enzymes. Cell reports **42**(6) (2023)

[103] Gooptu, B.: Surfactant protein c mutations and familial pulmonary fibrosis: stuck in a loop on the scenic route. European Respiratory Journal **59**(1) (2022) https://doi.org/10.1183/13993003.02147-2021 https://publications.ersnet.org//content/erj/59/1/2102147.full.pdf

[104] Nakanishi, T., Forgetta, V., Handa, T., Hirai, T., Mooser, V., Lathrop, G.M., Cookson, W.O.C.M., Richards, J.B.: The undiagnosed disease burden associated with alpha-1 antitrypsin deficiency genotypes. European Respiratory Journal **56**(6) (2020) https://doi.org/10.1183/13993003.01441-2020 https://publications.ersnet.org//content/erj/56/6/2001441.full.pdf

[105] Fromme, M., Schneider, C.V., Pereira, V., Hamesch, K., Pons, M., Reichert, M.C., Benini, F., Ellis, P., H Thorhauge, K., Mandorfer, M., Burbaum, B., Woditsch, V., Chorostowska-Wynimko, J., Verbeek, J., Nevens, F., Genesca, J., Miravitlles, M., Nuñez, A., Schaefer, B., Zoller, H., Janciauskiene, S., Abreu, N., Jasmins, L., Gaspar, R., Liberal, R., Macedo, G., Mahadeva, R., Gomes, C., Schneider, K.M., Trauner, M., Krag, A., Gooptu, B., Thorburn, D., Marshall, A., Hurst, J.R., Lomas, D.A., Lammert, F., Gaisa, N.T., Clark, V., Griffiths, W., Trautwein, C., Turner, A.M., McElvaney, N.G., Strnad, P.: Hepatobiliary phenotypes of adults with alpha-1 antitrypsin deficiency. Gut **71**(2), 415–423 (2022) https://doi.org/10.1136/gutjnl-2020-323729 https://gut.bmj.com/content/71/2/415.full.pdf

[106] Le, A., Ferrell, G.A., Dishon, D.S., Le, Q.Q.A., Sifers, R.N.: Soluble aggregates of the human piz 1-antitrypsin variant are degraded within the endoplasmic reticulum by a mechanism sensitive to inhibitors of protein synthesis. Journal of Biological Chemistry **267**, 1072–1080 (1992) https://doi.org/10.1016/s0021-9258(18)48397-4

[107] Cabral, C.M., Liu, Y., Moremen, K.W., Sifers, R.N.: Organizational diversity among distinct glycoprotein endoplasmic reticulum-associated degradation programs. Molecular Biology of the Cell **13**(8), 2639–2650 (2002) https://doi.org/10.1091/mbc.e02-02-0068 https://doi.org/10.1091/mbc.e02-02-0068. PMID: 12181335

[108] Kroeger, H., Miranda, E., MacLeod, I., Pérez, J., Crowther, D.C., Marciniak, S.J., Lomas, D.A.: Endoplasmic reticulum-associated degradation (erad) and autophagy cooperate to degrade polymerogenic mutant serpins *. Journal of Biological Chemistry **284**, 22793–22802 (2009) https://doi.org/10.1074/jbc.M109.027102 . doi: 10.1074/jbc.M109.027102

[109] Bouchecareilh, M., Hutt, D.M., Szajner, P., Flotte, T.R., Balch, W.E.: Histone deacetylase inhibitor (hdaci) suberoylanilide hydroxamic acid (saha)-mediated correction of 1-antitrypsin deficiency *. Journal of Biological Chemistry **287**, 38265–38278 (2012) https://doi.org/10.1074/jbc.M112.404707 . doi: 10.1074/jbc.M112.404707

[110] Minh, B.Q., Schmidt, H.A., Chernomor, O., Schrempf, D., Woodhams, M.D., Haeseler, A., Lanfear, R.: Iq-tree 2: New models and efficient methods for phylogenetic inference in the genomic era. Mol Biol Evol **37**(5), 1530–1534 (2020) https://doi.org/10.1093/molbev/msaa015

[111] Letunic, I., Bork, P.: Interactive tree of life (itol) v6: recent updates to the phylogenetic tree display and annotation tool. Nucleic Acids Res **52**(W1), 78–82 (2024) https://doi.org/10.1093/nar/gkae268

[112] Altschul, S.F., Gish, W., Miller, W., Myers, E.W., Lipman, D.J.: Basic local alignment search tool. Journal of Molecular Biology **215**(3), 403–410 (1990) https://doi.org/10.1016/S0022-2836(05)80360-2

[113] Robert, X., Gouet, P.: Deciphering key features in protein structures with the new ENDscript server. Nucleic Acids Research **42**(W1), 320–324 (2014) https://doi.org/10.1093/nar/gku316 https://academic.oup.com/nar/article-pdf/42/W1/W320/17422987/gku316.pdf

[114] Heckman, K.L., Pease, L.R.: Gene splicing and mutagenesis by pcr-driven overlap extension. Nature Protocols **2**, 924–932 (2007) https://doi.org/10.1038/nprot.2007.132

[115] Feliciello, I., Chinali, G.: A modified alkaline lysis method for the preparation

of highly purified plasmid dna from escherichia coli. Analytical Biochemistry **212**(2), 394–401 (1993) https://doi.org/10.1006/abio.1993.1346

[116] Portolano, N., Watson, P.J., Fairall, L., Millard, C.J., Milano, C.P., Song, Y., Cowley, S.M., Schwabe, J.W.R.: Recombinant protein expression for structural biology in HEK 293f suspension cells: A novel and accessible approach. Journal of Visualized Experiments (92) (2014) https://doi.org/10.3791/51897

[117] Bokori-Brown, M., Martin, T.G., Naylor, C.E., Basak, A.K., Titball, R.W., Savva, C.G.: Cryo-em structure of lysenin pore elucidates membrane insertion by an aerolysin family protein. Nature Communications **7** (2016) https://doi.org/10.1038/ncomms11293

[118] Kimanius, D., Dong, L., Sharov, G., Nakane, T., Scheres, S.H.W.: New tools for automated cryo-EM single-particle analysis in RELION-4.0. Biochemical Journal **478**(24), 4169–4185 (2021) https://doi.org/10.1042/BCJ20210708

[119] Punjani, A., Rubinstein, J.L., Fleet, D.J., Brubaker, M.A.: Cryosparc: Algorithms for rapid unsupervised cryo-em structure determination. Nature Methods **14**, 290–296 (2017) https://doi.org/10.1038/nmeth.4169

[120] Zheng, S., Palovcak, E., Armache, J.-P., Cheng, Y., Agard, D.: Anisotropic Correction of Beam-induced Motion for Improved Single-particle Electron Cryo-microscopy. bioRxiv, 1–30 (2016)

[121] Rohou, A., Grigorieff, N.: CTFFIND4: Fast and accurate defocus estimation from electron micrographs. Journal of Structural Biology **192**(2), 216–221 (2015) https://doi.org/10.1016/j.jsb.2015.08.008

[122] Bepler, T., Kelley, K., Noble, A.J., Berger, B.: Topaz-Denoise: general deep denoising models for cryoEM and cryoET. Nature Communications **11**(1) (2020) https://doi.org/10.1038/s41467-020-18952-1

[123] Goddard, T.D., Huang, C.C., Meng, E.C., Pettersen, E.F., Couch, G.S., Morris, J.H., Ferrin, T.E.: UCSF ChimeraX: Meeting modern challenges in visualization and analysis. Protein Science **27**(1), 14–25 (2018) https://doi.org/10.1002/pro.3235

[124] Punjani, A., Fleet, D.J.: 3D variability analysis: Resolving continuous flexibility and discrete heterogeneity from single particle cryo-EM. Journal of Structural Biology **213**(2), 107702 (2021) https://doi.org/10.1016/j.jsb.2021.107702

[125] Evans, R., O'neill, M., Pritzel, A., Antropova, N., Senior, A., Green, T., Žídek, A., Bates, R., Blackwell, S., Yim, J., Ronneberger, O., Bodenstein, S., Zielinski, M., Bridgland, A., Potapenko, A., Cowie, A., Tunyasuvunakool, K., Jain, R., Clancy, E., Kohli, P., Jumper, J., Hassabis, D.: Protein complex prediction with alphafold-multimer. bioRxiv (2022) https://doi.org/10.1101/2021.10.04.463034

[126] Liebschner, D., Afonine, P.V., Baker, M.L., Bunkoczi, G., Chen, V.B., Croll, T.I., Hintze, B., Hung, L.W., Jain, S., McCoy, A.J., Moriarty, N.W., Oeffner, R.D., Poon, B.K., Prisant, M.G., Read, R.J., Richardson, J.S., Richardson, D.C., Sammito, M.D., Sobolev, O.V., Stockwell, D.H., Terwilliger, T.C., Urzhumtsev, A.G., Videau, L.L., Williams, C.J., Adams, P.D.: Macromolecular structure determination using X-rays, neutrons and electrons: Recent developments in Phenix. Acta Crystallographica Section D: Structural Biology **75**, 861–877 (2019) https://doi.org/10.1107/S2059798319011471

[127] Afonine, P.V., Poon, B.K., Read, R.J., Sobolev, O.V., Terwilliger, T.C., Urzhumtsev, A., Adams, P.D.: Real-space refinement in PHENIX for cryo-EM and crystallography. urn:issn:2059-7983 **74**(6), 531–544 (2018) https://doi.org/10.1107/S2059798318006551

[128] Emsley, P., Cowtan, K.: Coot: Model-building tools for molecular graphics. Acta Crystallographica Section D: Biological Crystallography **60**(12 I), 2126–2132 (2004) https://doi.org/10.1107/S0907444904019158

[129] Casañal, A., Lohkamp, B., Emsley, P.: Current developments in Coot for macromolecular model building of Electron Cryo-microscopy and Crystallographic Data. Protein Science **29**(4), 1069–1078 (2020) https://doi.org/10.1002/pro.3791

[130] Clough, S.J., Bent, A.F.: Floral dip: a simplified method forAgrobacterium-mediated transformation ofArabidopsis thaliana. The Plant Journal **16**(6), 735–743 (1998) https://doi.org/10.1046/j.1365-313x.1998.00343.x

[131] McNicholas, S., Agirre, J.: Glycoblocks: a schematic three-dimensional representation for glycans and their interactions. Acta crystallographica. Section D, Structural biology **73**(Pt 2), 187–194 (2017)